

Thermal Analysis

Information for Users



31 User Com

Dear Customer,

In recent years, modern scientific instruments have become more and more powerful, not least due to excellent software. However, less and less time is available for training and performing daily analytical tasks.

We are aware of this problem and do our utmost to support you in these areas. Besides our classical training courses, we offer a variety of handbooks and literature for self-study. The latest addition to this training program is a series of webinars that enable you to learn about new applications, methods and techniques in thermal analysis conveniently via Internet.

On the same topic, we are also delighted to announce the availability of another new handbook in the Collected Applications series. The handbook is entitled "Thermal Analysis in Practice" and is described in detail in the News section. It should be of great help as a practical guide and reference in your daily work.

Thermal analysis of polymers. Part 1: DSC of thermoplastics

Dr. Angela Hammer

This is the first of a series of six articles on the thermal analysis of polymers. The aim is to demonstrate and explain the various effects that can be measured by thermal analysis to characterize samples. The experiments have been performed using three different types of plastic materials, namely a thermoplastic (PET), a thermoset (KU 600), and an elastomer (W001). Thermal analysis is widely used in the polymer, petrochemical, chemical, pharmaceutical, automotive, microelectronics, food, and cosmetics industries as well as in scientific research.

Contents 1/2010

TA Tip

- Thermal analysis of polymers.
Part 1: DSC of thermoplastics 1

New in our Sales Program

- The new comprehensive thermal analysis handbook 7
- Melting point software, Version 1.1 8

Applications

- Curing kinetics of EVA using DSC, DMA and model free kinetics 9
- UV curing of a cycloaliphatic epoxy resin using TOPEM® and conventional DSC 13
- Analysis of the components of a sandwich composite panel by DMA 17
- TGA/MaxRes used for studies on hydrogen storage 20

Dates

- Exhibitions 23
- Courses and Seminars 23

METTLER TOLEDO

Introduction

Thermal analysis encompasses a group of techniques that are used to measure the physical properties of a substance as a function of time while the substance is subjected to a controlled temperature program. The techniques include DSC (Differential Scanning Calorimetry), TGA (Thermogravimetric Analysis), TMA (Thermomechanical Analysis) and DMA (Dynamic Mechanical Analysis).

Thermal analysis is employed in research and development, process optimization, quality control, material failure and damage analysis as well as to analyze competitive products. For example, the influence of moisture content, additives, plasticizers or fillers, and the content of impurities and contaminants can be determined from thermal measurements.

Furthermore, the different methods yield information about the processing, thermal history and pretreatment (storage and use), mechanical stress or strain, and dimensional changes.

This first article describes how DSC is used to analyze a thermoplastic, PET (polyethylene terephthalate), as comprehensively as possible [1]. The results

of the various methods are compared with one another. The main topics discussed are:

- Glass transition
- Cold crystallization
- Recrystallization
- Melting
- Thermal history
- Oxidation induction time
- Decomposition.

PET

PET was chosen to represent the group of thermoplastic polymers. It is a polyester produced in a polycondensation reaction between terephthalic acid and ethylene glycol. Its structure is shown in Figure 1.

PET is used for many different applications. One of the most well known is the manufacture of plastic bottles in the beverage industry. It is also used as a fiber in the sports clothing industry because of its excellent crease-, tear- and weather-resistance properties and low water absorption.

Films of 1 to 500 μm are used for packaging materials, for the manufacture of furniture, sunshades, and so on. The finished films are often coated or laminated with other films and are widely used in the food industry, for example for packaging coffee or other foodstuffs to prevent the loss of aroma. The characterization of the properties of the material is therefore very important in order to guarantee constant quality.

Experimental details

The DSC measurements described in this article were performed using a DSC 1 equipped with an FRS5 sensor and evaluated with the STAR[®] software.

PET samples weighing about 3 to 10 mg were prepared and pretreated depending on the application. In general, samples should have a flat surface and make good contact with the crucible. The bottom of the crucible should not be deformed by the sample material when it is sealed.

Measurements and results

Differential scanning calorimetry

DSC is a technique that measures the heat flow of samples as a function of temperature or time. The method allows physical transitions and chemical reactions to be quantitatively measured [2].

Effects of this type will be analyzed with the aid of different DSC measurements. Figure 2 shows the most important events that occur when PET is measured by DSC. These are often characteristic for a substance and serve as a fingerprint, enabling them to be used for quality control.

Figure 2 displays a typical first heating measurement curve of a PET sample. It shows the glass transition, cold crystallization, and melting. The glass transition exhibits enthalpy relaxation, which is shown by the overlapping endothermic peak. The latter occurs when the sample has been stored for a long time at a temperature below the glass transition. Cold crystallization takes place when the sample is cooled rapidly and has no time to crystallize during the cooling phase. The DSC curve can also be used to determine the specific heat capacity, c_p . Different standard procedures exist for the determination of the glass transition temperature; several of these are evaluated directly by the STAR[®] software and are shown in Figure 2.

Glass transition

The glass transition is a reversible transition that occurs when an amorphous material is heated or cooled in a particular temperature range. It is character-

Figure 1. Structural formula of PET.

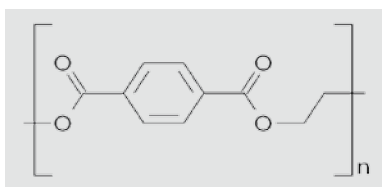
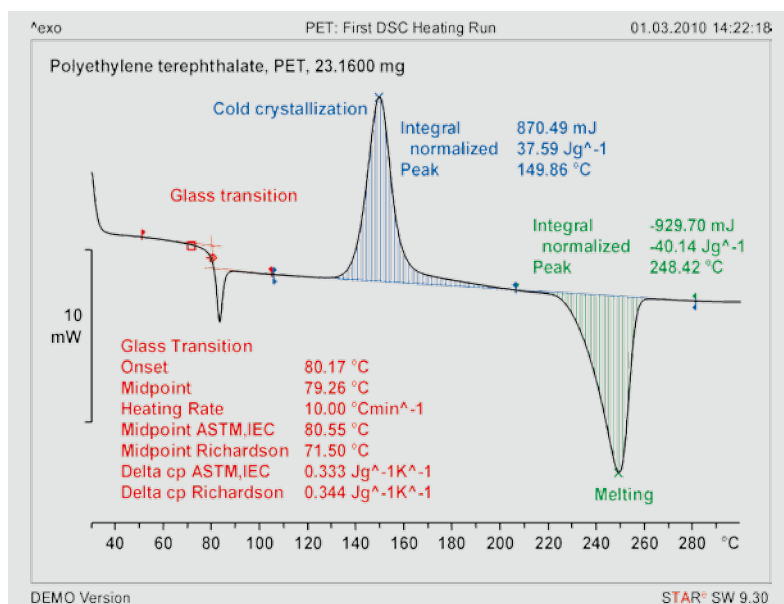


Figure 2. The main effects measured by DSC using PET as a sample. Temperature range 30–300 °C; heating rate 20 K/min; purge gas nitrogen at 50 mL/min.



ized by the glass transition temperature, T_g . On cooling, the material becomes brittle (less flexible) like a glass, and on heating becomes soft [2, 3, 4, 5]. In the case of thermoplastics, the glass transition correlates with the region above which the material can be molded. The glass transition is exhibited by semicrystalline or completely amorphous solids as well as by ordinary glasses and plastics (organic polymers). Above the glass transition, glasses or organic polymers become soft and can be plastically deformed or molded without breaking. This behavior is one of the properties that makes plastics so useful.

The glass transition is a kinetic phenomenon; the measured value of the glass transition depends on the cooling rate, the thermomechanical history of the sample and the evaluation conditions. The lower the cooling rate, the lower the resulting glass transition that is measured in the following heating run. This means that the glass transition temperature depends on the measurement conditions and cannot be precisely defined.

In many cases, an enthalpy relaxation peak is observed that overlaps the glass transition. This depends on the history of the sample. Physical aging below the glass transition leads to enthalpy relaxation.

At the glass transition temperature, T_g , the following physical properties change:

- Specific heat capacity (c_p)
- Coefficient of Thermal Expansion, CTE, (can be measured by TMA)
- Mechanical modulus (can be measured by DMA)
- Dielectric constant

The 2/3 rule can be used as a rule of thumb. This states that the glass transition temperature corresponds to 2/3 of the melting point temperature (in Kelvin):

- For PET: T_{melt} is 256 °C or 529.16 K
- $T_g \sim 352.8$ K or 79.6 °C

The glass transition appears as a step in the DSC curve and shows the change of the specific heat capacity, c_p , from the solid to the liquid phase.

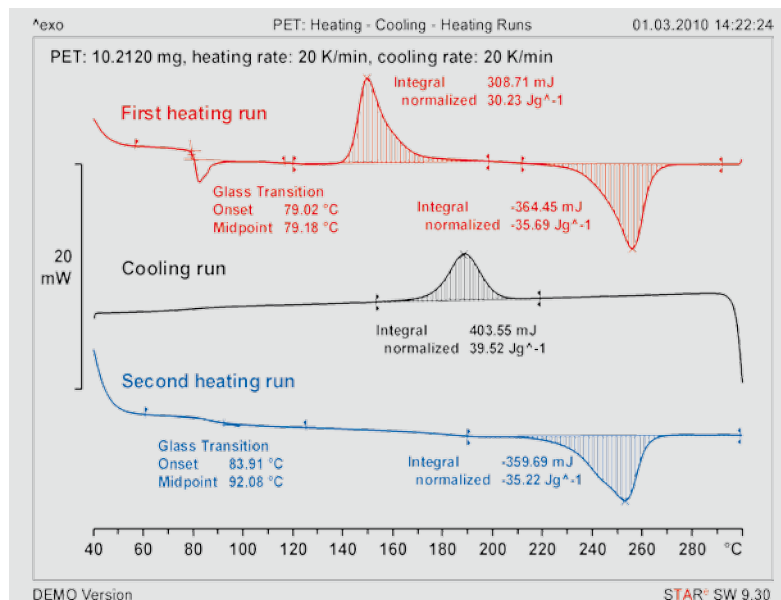


Figure 3. First and second heating runs and the cooling curve demonstrate differences regarding relaxation at the glass transition and the disappearance of cold crystallization.

Cold crystallization

Cold crystallization is an exothermic crystallization process. It is observed on heating a sample that has previously been cooled very quickly and has had no time to crystallize. Below the glass transition, molecular mobility is severely restricted and cold crystallization does not occur; above the glass transition, small crystallites are formed at relatively low temperatures. The process is called cold crystallization.

Melting

Melting is the transition from the solid to the liquid state. It is an endothermic process and occurs at a defined temperature for pure substances. The temperature remains constant during the transition: The heat supplied is required to bring

about the change of state and is known as the latent heat of melting.

Crystallinity

The degree of crystallinity is the percentage crystalline content of a semicrystalline substance. Thermoplastics normally exhibit a degree of crystallinity of up to 80%. The degree of crystallinity of a material depends on its thermal history. It can be determined by measuring the enthalpy of fusion of the sample and dividing this by the enthalpy of fusion of the 100% crystalline material. 100% crystalline materials can be determined X-ray diffraction.

Semicrystalline samples such as PET undergo cold crystallization above their glass transition. This makes it difficult to determine their degree of crystallinity

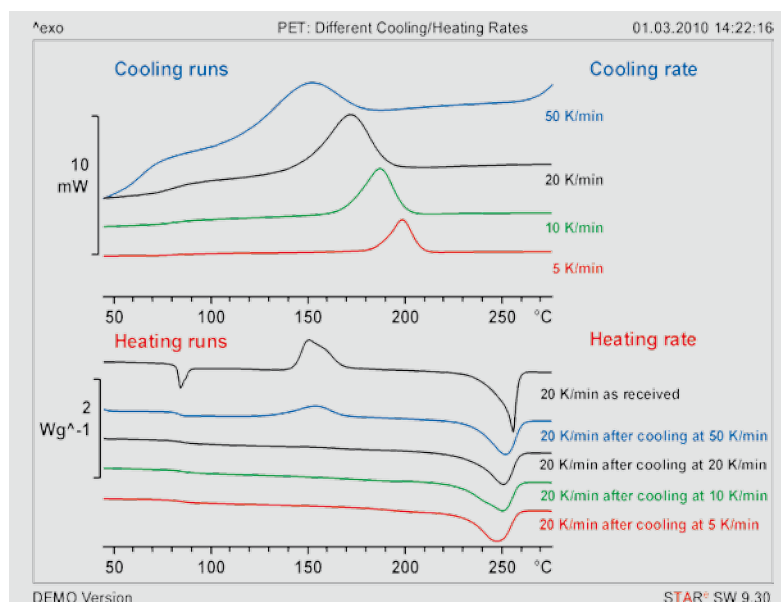


Figure 4. DSC measurements of the same sample performed at different cooling rates. At low cooling rates, cold crystallization cannot be detected on heating because sufficient time was available for crystallization to occur during cooling.

before the measurement. This particular topic will therefore not be further discussed in this article.

Recrystallization

Recrystallization is a type of reorganization process in which larger crystallites are formed from smaller crystallites. The process is heating-rate dependent: the lower the heating rate, the more time there is for reorganization. Recrystallization is difficult to detect by DSC because exothermic crystallization and endothermic melting occur simultaneously.

Heating-Cooling-Heating

Figure 3 shows a measurement in which a sample was heated, cooled, and then heated again at 20 K/min. This type of experiment is often performed to ther-

mally pretreat the sample in a defined way in the first heating run. In Figure 3, the first heating run corresponds to the curve shown in Figure 2. The figure also shows that the second heating run is very different to the first run – the melting peak is broader and the relaxation at the glass transition and the cold crystallization are no longer present. During cooling the sample had sufficient time for crystallization to occur. The crystallization peak is clearly visible in the cooling curve. Since the sample was heated immediately afterward, no enthalpy relaxation occurs because it had no time to undergo physical aging.

In practice, heating-cooling-heating experiments are used to eliminate the thermal history of material and to check the

production process of a sample. In the second heating run, the glass transition step is smaller. This means that the content of amorphous material is lower and the crystalline content larger than in the first heating run. Crystallization results in a decrease in the amorphous content and a corresponding increase in the degree of crystallinity.

Different cooling rates

Figure 4 shows the influence of different cooling rates on crystallization and the temperature range in which crystallization occurs. The higher the cooling rate, the more the crystallization peak is shifted to lower temperatures. When the sample is cooled very slowly, cold crystallization is not observed in the heating run performed immediately afterward. In contrast, if the sample is cooled rapidly, it has no time to crystallize and cold crystallization is observed when the sample is heated. For example, if PET is cooled at 50 K/min, the sample cannot crystallize completely. As a result, the amorphous part of the sample exhibits cold crystallization in the following heating run.

Thermal history

Figure 5 illustrates the influence of the thermal history on a PET sample. The sample was cooled under different conditions: first cooled very slowly, second shock cooled, and third shock cooled and annealed at 65 °C for ten hours, that is, stored at a temperature somewhat below that of the glass transition temperature. The heating measurements performed after each cooling run show clear differences.

The sample that was slowly cooled shows only a small step at the glass transition and no cold crystallization – sufficient time was available for the sample to crystallize and so the content of amorphous material is low. The shock-cooled sample shows a large glass transition step. This indicates that the amorphous content is high. Furthermore, a cold crystallization peak is observed because the sample did not have sufficient time to crystallize. The sample annealed at 65 °C for ten hours exhibits enthalpy relaxation as a result of the aging process in addition to the effects seen in the shock-cooled

Figure 5. Heating curves of a PET sample after cooling under different conditions.

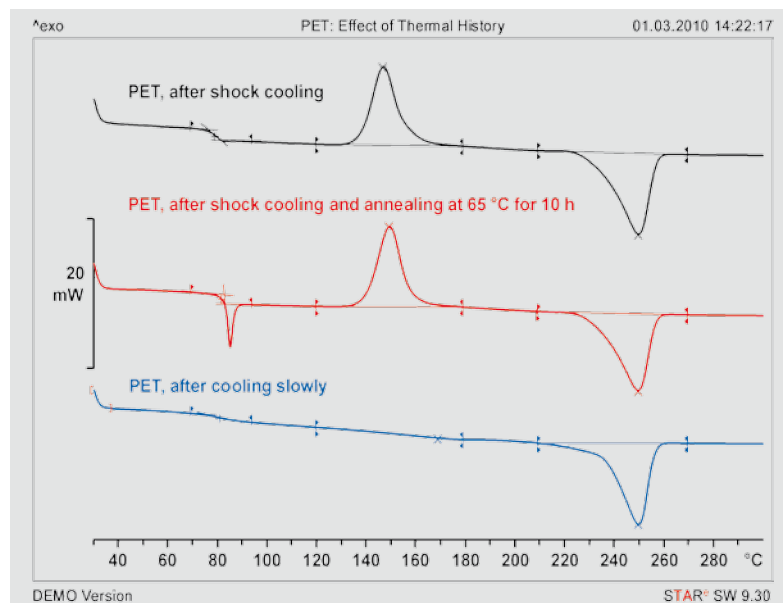
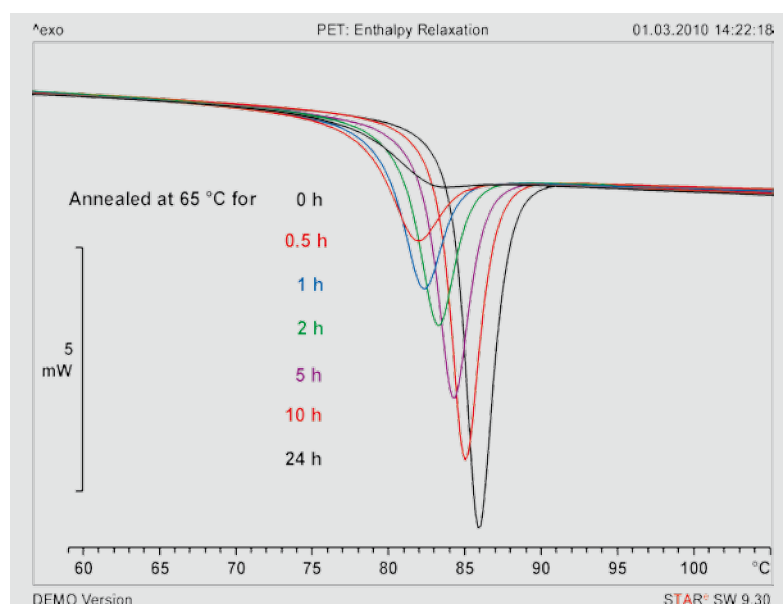


Figure 6. Heating runs showing the influence of different annealing times on the glass transition and the enthalpy relaxation peak of PET.



sample. The melting peaks of the three samples are almost identical. The melting peak does not seem to be influenced by the thermal pretreatment.

Figure 6 shows the influence of different annealing times on enthalpy relaxation. The sample was first heated from 30 to 300 °C at a heating rate of 10 K/min and then shock cooled and annealed at 65 °C for different times (0 to 24 h). The measurements were performed from 30 to 300 °C at a heating rate of 10 K/min.

The longer a sample is stored below the glass transition, the greater the enthalpy relaxation and the more pronounced the effect of physical aging. The enthalpy relaxation peak is often a result of the thermal history of a sample and affects the evaluation of the glass transition. The peak can be eliminated by first heating the sample to a temperature slightly above the glass transition, shock cooling it and then heating it a second time. In fact, enthalpy relaxation contains valuable information about the thermal and mechanical history of a sample (storage temperature, storage time, cooling rate, etc.). In practice, the temperature at which samples or materials are stored is an important factor that should be taken into account in order to prevent undesired physical aging.

Heating rates

Figure 7 illustrates the influence of different heating rates on the DSC measurement of PET samples [6, 7]. The higher the heating rate, the less time there is for crystallization. At 300 K/min, the sample has no time to crystallize and consequently shows no melting peak.

TOPEM®

TOPEM® is the newest and most powerful temperature-modulation technique used in DSC alongside IsoStep and ADSC. It allows reversing and non-reversing effects to be separated from each other.

Figure 8 shows the results obtained from a TOPEM® measurement of PET using standard parameters. The sample was preheated to 80 °C and shock cooled by removing the crucible from the furnace and placing it on a cold aluminum

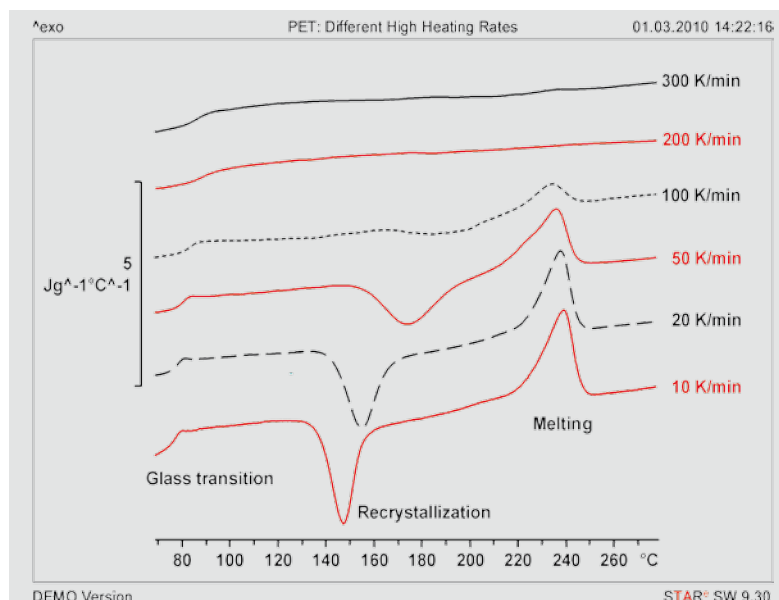


Figure 7. DSC measurements of PET at high heating rates, shown as c_p curves.

plate. The TOPEM® experiment was performed in a 40- μ L aluminum crucible with a hole in the lid at a heating rate of 0.2 K/min.

The uppermost curve in Figure 8 shows the measurement data before evaluation. The TOPEM® evaluation yields separate curves for the total heat flow (black), reversing heat flow curve (red) and the non-reversing heat flow curve (blue). In addition, the quasi-static c_{p0} can be calculated from the measurement. In a second step, the heat capacity or phase can be determined at user-defined frequencies. In Figure 8, this is done at a frequency of 16.7 Hz. TOPEM® [8, 9] is also an excellent technique to determine c_p and to separate effects that cannot be separated by DSC. For example, it can separate the enthalpy change associated with a glass

transition from the enthalpy produced in a reaction that occurs simultaneously – a glass transition is a reversing effect while a reaction is a non-reversing effect.

The TOPEM® technique uses a stochastic temperature profile. This allows the sample to be characterized from the results of just one single measurement. The curves in Figure 9 show the frequency dependence of the glass transition of a sample of PET. In this case, the glass transition shifts to higher temperature at higher frequencies. In contrast, the step in the curve due to cold crystallization occurs at the same temperature and is independent of frequency. The frequency dependence of certain effects shown by unknown substances can thus be studied in order to clarify the interpretation of their origin.

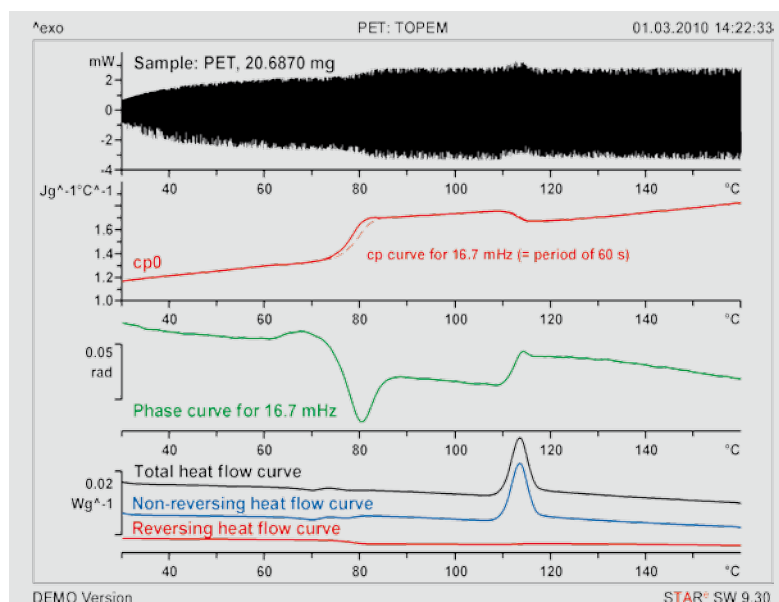


Figure 8. Measurement of a PET sample using TOPEM® showing the reversing, non-reversing and total heat flow curves.

Oxidative stability (OIT/OOT)

Finally, we would like to briefly explain two DSC methods known as OIT and OOT that are used to measure the oxidative stability [10, 11] of polymers and oils. The methods simulate the accelerated chemical aging of products and allow information to be obtained about their relative stability. For example, different materials can be compared with one another or samples of the same material containing different additives can be analyzed to determine the influence of an additive. In practice, the method is widely used for PE (polyethylene). The application example described below also uses a sample of PE because the decom-

position of PET is overlapped by melting and re-esterification and cannot be clearly identified.

The OIT (Oxidation Induction Time) measurement of PE (Figure 10) is often performed in crucibles made of different metals in order to determine the influence of the particular metal on the stability of the PE. In this example, the measurement was started in a nitrogen atmosphere according to the following temperature program: 3 min at 30 °C, heating at 20 K/min from 30 to 180 °C, then isothermal at 180 °C. After 2 min the gas was switched to oxygen. The measurement was stopped as soon as

oxidation was observed. The OIT is the time interval from when the purge gas is switched to oxygen to the onset of oxidation. Measurements were performed in open 40- μ L aluminum and copper crucibles for comparison. Oxidation clearly takes place much earlier in the copper crucible than in the aluminum crucible. The copper acts as a catalyst and accelerates the decomposition of PE.

The oxidative stability of samples can also be compared by measuring the Onset Oxidation Temperature (OOT). In this method, the sample is heated in an oxygen atmosphere and the onset temperature at which oxidation begins is evaluated.

Since OIT measurements are easy to perform and do not take much time, they are often used in quality control to compare the stability of products.

Part 2 of this series of articles dealing with TGA, TMA, and DMA measurements of thermoplastics will appear in UserCom 32.

Figure 9. Measurement of a PET sample using TOPEM® showing the frequency dependence of the glass transition.

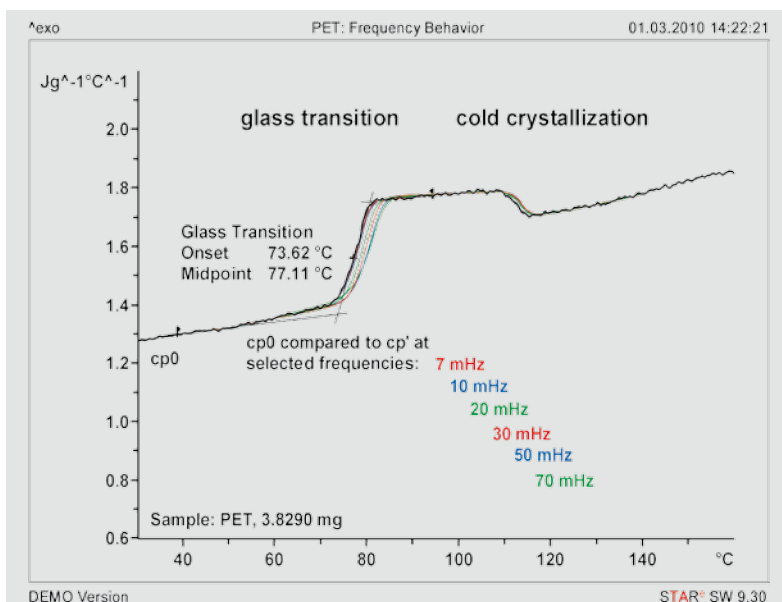
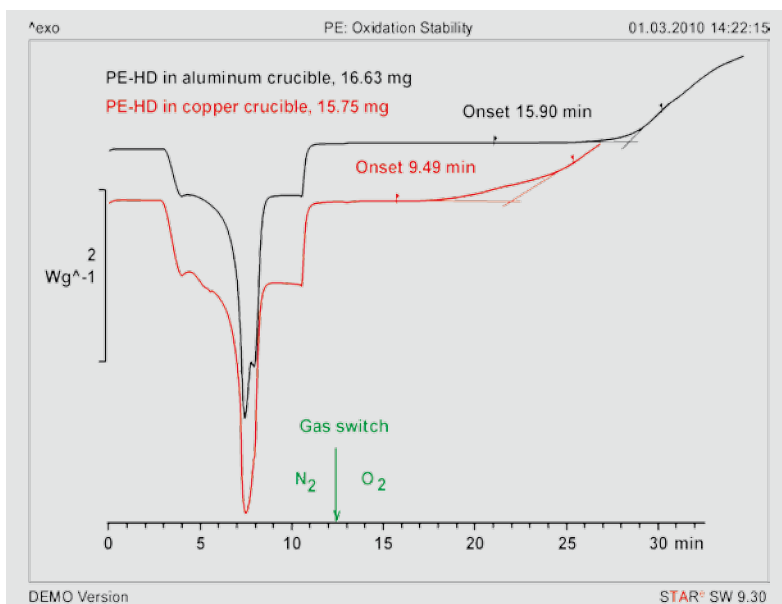


Figure 10. OIT measurements of PE in different crucibles.



References

- [1] Total Analysis with DSC, TMA and TGA-EGA, UserCom 9, 8–12.
- [2] Interpreting DSC curves, Part 1: Dynamic measurements, UserCom 11, 1–7.
- [3] The glass transition from the point of view of DSC-measurements; Part 1: Basic principles, UserCom 10, 13–16.
- [4] The glass transition temperature measured by different TA techniques, Part 1: Overview, UserCom 17, 1–4.
- [5] R. Riesen, The glass transition temperature measured by different TA technique, Part 2: Determination of glass transition temperatures, UserCom 18, 1–5.
- [6] M. Wagner, DSC Measurements at high heating rates – advantages and limitations, UserCom 19, 1–5.
- [7] R. Riesen, Influence of the heating rate: Melting and chemical reactions, UserCom 23, 20–22.
- [8] TOPEM® – The new multi-frequency temperature-modulated technique, UserCom 22, 6–8.
- [9] J. Schawe, Analysis of melting processes using TOPEM®, UserCom 25, 13–17.
- [10] Oxidative stability of petroleum oil fractions, UserCom 10, 7–8.
- [11] A. Hammer, The characterization of olive oils by DSC, UserCom 28, 6–8.

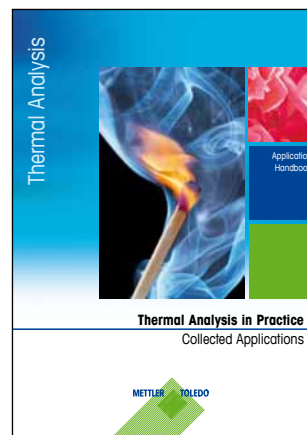
The new comprehensive thermal analysis handbook

Training has always been a very important topic in thermal analysis. Only well-trained users can measure samples properly, and correctly interpret and evaluate the results.


We are delighted to announce the new Thermal Analysis in Practice handbook comprising some 20 chapters and 327 pages. The handbook presents practical and theoretical aspects of the DSC, TGA, TMA, and DMA techniques and includes a large number of practical examples.

There are separate chapters on the glass transition, polymers, polymorphism, purity determination, and method development. The chapters are independent of one another and can be read individually in any desired order.

The handbook is suitable both for training purposes and as a reference manual. Newcomers can rapidly learn the basic principles of thermal analysis while experienced users can take advantage of a vast reservoir of knowledge and experience.



METTLER TOLEDO supports you in thermal analysis training in many other ways:

Product	Purpose	Further information
Thermal Analysis in Practice handbook ME 51 725 244 (in English only).	For training, further education, and reference.	You can have a look at the handbook at www.mt.com/ta-handbooks .
Tutorial Kit  Handbook with test substances: ME 51 140 878 (in English) ME 51 140 877 (in German) ME 51 140 879 (in French)	The Tutorial Kit is an excellent way to learn thermal analysis. Each of the well-chosen 14 test substances has been measured using one of the main thermal analysis techniques. The measurements are fully evaluated and documented.	
Thermal analysis courses	For training and/or further education.	See the current course program on the final pages.
UserCom	The bi-annual publication contains many practical tips and application examples from widely different fields.	www.mt.com/ta-UserComs allows you to access previous issues. You can also register for your own personal copy of UserCom.
Webinars	Provide an introduction into selected topics in thermal analysis.	www.mt.com/ta-webinars presents an overview of our current webinar program.
Thermal analysis handbooks cover the most important types of materials and topics in thermal analysis. (in English only)	For further study in special application fields.	www.mt.com/ta-handbooks gives an overview of our current series of thermal analysis handbooks.

www.mt.com/ta-news presents an overview of METTLER TOLEDO Thermal Analysis Excellence with links to training courses, new products, and special promotions.

Similarly at www.mt.com/fp-news you can get an overview of our new products and special offers in the Thermal Values product line.

Melting point software, Version 1.1

A new software update is now available for the Excellence Melting Point Systems (MP Update 1.1).

Many new functions have been incorporated following customer feedback and requests.

The table presents an overview of the most important new features.

New instruments will be delivered with the new software.

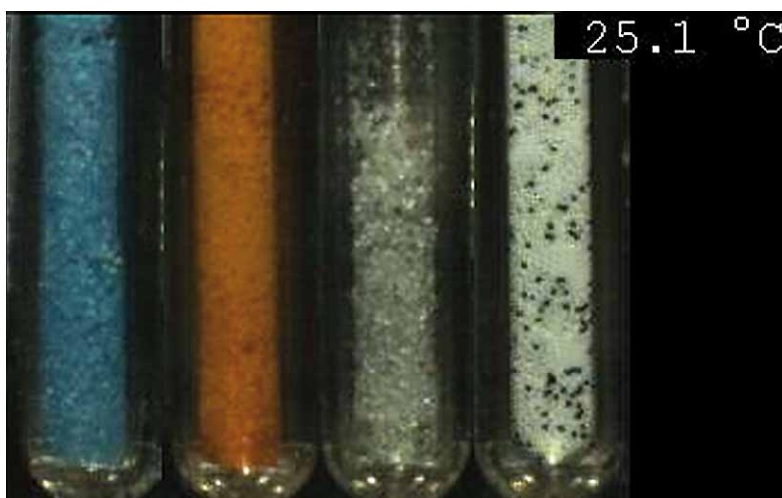
Existing users can easily download and install the software update after registering at www.mt.com/thermal-values-update.

Operating instructions are supplied with the download.

Do not forget to make a backup copy of your data beforehand.

Figure 1.
An image extracted from an MP70 video showing the current temperature, above right. From left to right: copper sulfate pentahydrate, azobenzene, benzophenone and a mixture of 60- μm black and white polyethylene spheres.

Features and customer benefits	
User management with password protection and four fixed user levels	GMP-compliant access control
Network storage of result files	Greater flexibility. Allows transfer of PDF reports, ASCII files and for the MP90 videos directly to a PC without the need to handle the SD card
Temperature display in exported videos	Better traceability of results
Additional languages on the graphical user interface	Easier operation for users with Chinese, Japanese or Spanish mother tongue
Storage of results if the method is aborted	Saves time if melting has already occurred
Supports the METTLER TOLEDO keyboard and USB mouse devices	Entry of long texts is more convenient



Curing kinetics of EVA using DSC, DMA and model free kinetics

Klaus Wiegel, Gällivare PhotoVoltaic AB Företagscentrum, Box 840, SE-982 28 Gällivare, Sweden,
Dr. Angela Hammer and Dr. Markus Schubnell

The use of solar panels is well-known for converting sunlight to electricity. This so-called photovoltaic electrical power is expected to make an important contribution to providing a sustainable supply of energy in the future.

Introduction

A photovoltaic module consists of arrays of jointly connected solar cells. An important step in the manufacture of a photovoltaic module is encapsulation. In this production step, solar cells are encapsulated between a glass sheet and a Tedlar film as backing sheet.

Encapsulation is commonly performed using a 0.4-mm thick ethylene-vinyl acetate (EVA) film. It seals the module and protects it against environmental influences such as moisture, oxygen, and weathering. This is very important because a guaranteed lifetime of 25 years is

nowadays usual. In this article, we show how DSC and DMA experiments followed by evaluation with model free kinetics were used to investigate the curing behavior of EVA during the lamination process. Studies like this allow the optimum lamination conditions to be determined; the results can also be used for quality control.

In modern photovoltaic modules, the solar cells are encapsulated between a glass sheet and a backing sheet, usually a Tedlar® film [1, 2, 3], as illustrated in Figure 1. Sheets of ethylene-vinyl acetate (EVA) are placed between the solar cells

toward UV light, and electrical insulation. EVA is a block copolymer and in this application typically consists of 67% polyethylene and 33% vinyl acetate (see Figure 2). Uncured EVA is a thermoplastic material that on heating first exhibits a glass transition and then a melting process. In the curing process, the EVA chains undergo crosslinking. The curing reaction is initiated by a peroxide compound. This decomposes on heating and splits into two oxyradicals that promote the crosslinking of the EVA polymer. EVA only becomes mechanically and chemically resistant at the high temperatures that occur in photovoltaic modules (up to 80 °C) after this curing process.

It is important to determine the degree of cure of the EVA in order to optimize the lamination conditions and control the quality control of the finished photovoltaic modules. In the past, this was done using a method based on solvent extraction. Recently it was shown that DSC measurements can also be used [4].

In this article, we show how the curing reaction can be described by model free kinetics using data from DSC and DMA measurements. This allows the lamination process to be optimized with regard to temperature and lamination time.

Experimental details

Samples

The sample consisted of a piece of uncured EVA film, 0.4-mm thick, such as is used in the solar industry. Disks with a diameter of 3 mm were then punched out from this sample and used for the different experiments. The mass of a disk was typically about 5.8 mg.

Figure 1.
Construction of
a photovoltaic
module.

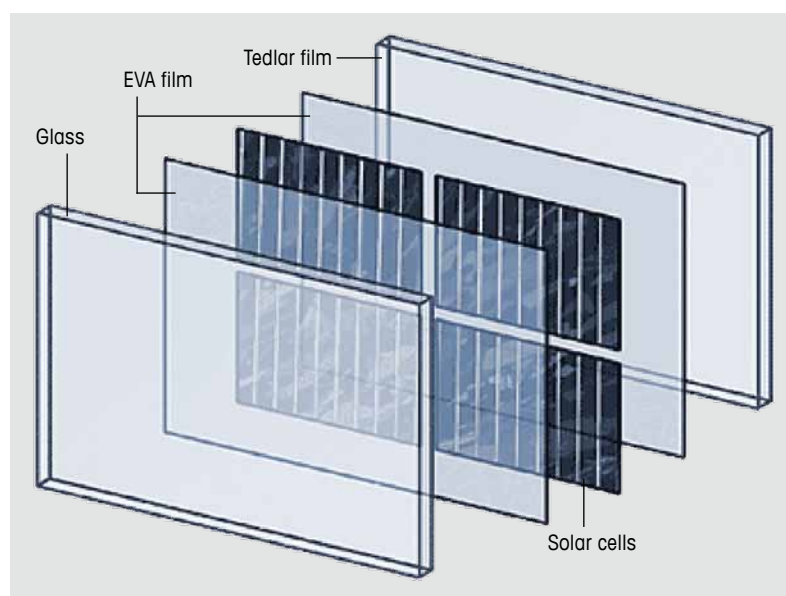
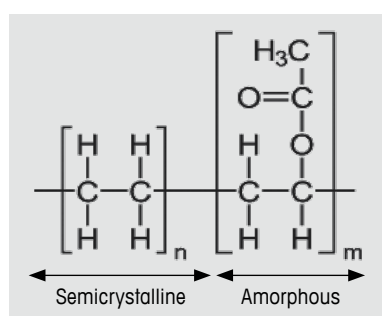


Figure 2.
Chemical structure
of EVA.



and the backing sheet and the glass. In the production process, the sandwich is pressed into place and heated. The EVA cures and provides a permanent and tight seal.

EVA has many excellent long-term properties such as its optical transmittance in the visible region, chemical resistance

DSC measurements

The DSC measurements were performed using a DSC 1 equipped with an Intra Cooler and an FRS5 sensor. The disks were measured in 40- μ L aluminum crucibles with a hole in the lid. The purge gas was nitrogen at 50 mL/min.

DMA measurements

The DMA measurements were performed in the shear mode using the DMA/SDTA861⁺. The maximum force and displacement amplitudes were 5 N and 5 μ m.

TGA measurements

The TGA measurements were performed using a TGA/DSC 1 equipped with a DTA sensor. The purge gas was nitrogen at 50 mL/min.

Results

DSC-and TGA experiments

Figure 3 shows the first and second DSC heating runs of EVA measured in the range -60 °C to 220 °C at a heating rate of 20 K/min. In the first heating run, the glass transition is clearly visible at about -30 °C. The sample then melts and the exothermic curing reaction occurs at about 170 °C. The glass transition is also observed in the second DSC heating run. The melting peak appears different because the thermal history of the sample was eliminated in the first heating run. An exothermic peak no longer occurs at 170 °C, which indicates that the sample reached its maximum degree of cure during the first heating run. The cool-

ing curve shows a very broad exothermic crystallization peak followed by the glass transition. The latter does not appear to be significantly influenced by the curing reaction.

The kinetics of the curing reaction was investigated using model free kinetics (MFK) [5, 6].

This method requires data from at least three experiments performed at different dynamic heating rates, in this case at 2 , 5 , and 10 K/min (Figure 4, above left). The corresponding conversion curves were then calculated from the DSC curves (Figure 4, below left) and the data used to calculate the activation energy as a function of the degree of conversion or curing (Figure 4, above right). The activation energy is used to make predictions about the degree of cure as a function of the curing time under isothermal conditions. This is illustrated in Figure 4 (below right) for a temperature of 135 °C. The curve measured in an isothermal DSC measurement performed at the same temperature is also shown. A comparison of the two curves shows that the MFK prediction agrees well with the experimental data.

A TGA measurement of an uncured EVA sample (Figure 5) showed that a small loss in weight of 0.66% occurred between 100 and 220 °C. This indicates that the decomposition reaction of the peroxide and the curing reaction of the EVA occur simultaneously. The DSC signal of the uncured EVA in this temperature range is therefore the sum of the decomposition reaction of the peroxide and the curing reaction of the EVA. The question therefore arose as to how accurately the kinetics of the curing reaction of EVA can be described by DSC. This led us to look for a method that is sensitive only to the curing reaction.

DMA experiments

During a curing reaction, molecules undergo crosslinking and form a network. The network density increases with increasing time (in an isothermal experiment) or with increasing temperature (in a dynamic experiment). For low network

Figure 3. EVA measured at 20 K/min: first heating run, the cooling curve, and the second heating run.

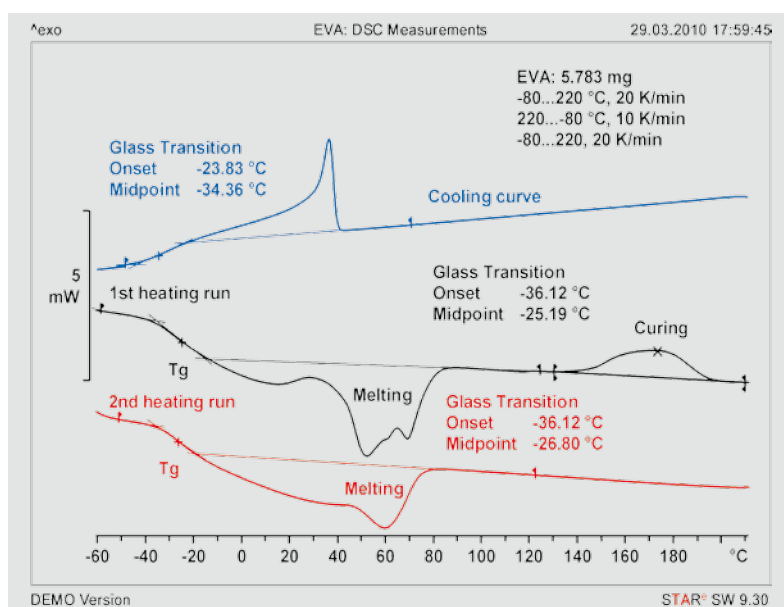
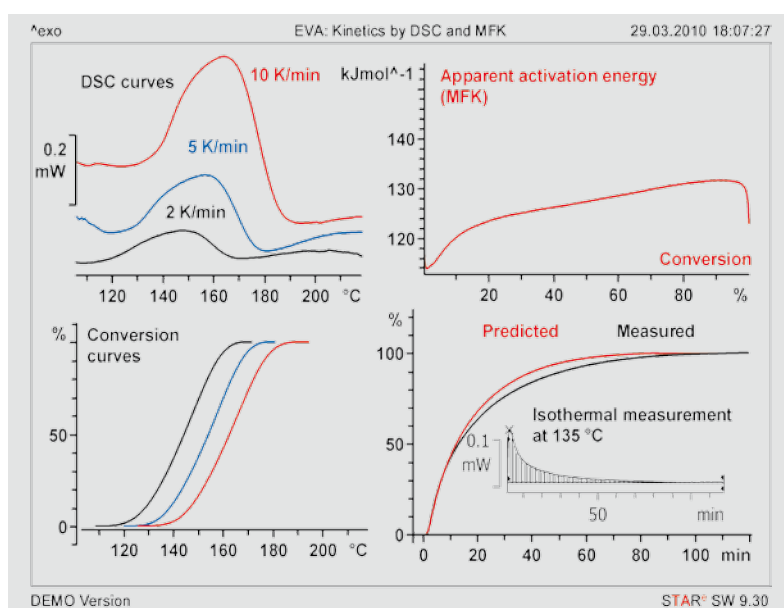


Figure 4. DSC/MFK evaluation. Above left: DSC heating curves. Below left: the calculated conversion curves. Above right: the apparent activation energy curves. Below right: predicted curve for isothermal curing at 135 °C and the isothermal measured curve.



densities (as in this case), the modulus is proportional to the network density. The curing process can therefore be studied by measuring the modulus, for example in a suitable DMA experiment, as illustrated in Figure 6.

The DMA measurements in the range $-60\text{ }^{\circ}\text{C}$ to $200\text{ }^{\circ}\text{C}$ show the storage modulus, G' , (the real component of the complex shear modulus), and the loss factor, $\tan\delta$, during the first and second heating runs. The first step in the storage modulus and the peak in $\tan\delta$ at about $-22\text{ }^{\circ}\text{C}$ correspond to the glass transition of the vinyl acetate (VA) part. The second step in the storage modulus at about $55\text{ }^{\circ}\text{C}$ is due to the melting of PE crystallites. During the first heating run, the sample becomes liquid at about $70\text{ }^{\circ}\text{C}$ ($\tan\delta > 1$). From about $120\text{ }^{\circ}\text{C}$ onward, the modulus increases and at the same time the loss factor decreases. This indicates that the material loses its liquid-like character and becomes rubbery ($\tan\delta \ll 1$) as a result of the beginning of the crosslinking reaction.

In the second heating run, the PE crystallites also melt at about $55\text{ }^{\circ}\text{C}$. However, they are now embedded in a crosslinked VA matrix, which gives the material a certain amount of mechanical stability. After melting, the loss factor therefore remains significantly smaller than in the first heating run. The crosslinking reaction leads to a slight increase in the modulus in the glassy state. The glass transition temperature of the crosslinked VA chains shows hardly any change compared with the glass transition temperature in the uncrosslinked state. This indicates that the degree of crosslinking is relatively low.

To apply model free kinetics to DMA data, the DMA measurements also have to be performed at different heating rates (see Figure 7, above left). Conversion curves for the curing reaction are then calculated from the DMA curves. This can be done by calculating the difference between the storage modulus at a particular temperature, $G'(T)$, and the modulus value before curing, G'_{bc} , ($123\text{ }^{\circ}\text{C}$ at a heating rate of 3 K/min) normalized to the

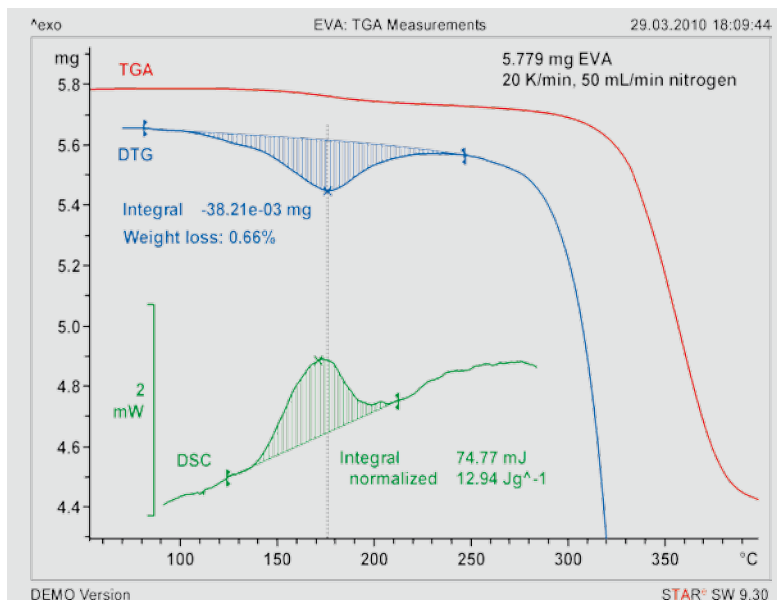


Figure 5. The TGA curve of uncured EVA shows a weight loss of about 0.66% between 100 and $250\text{ }^{\circ}\text{C}$.

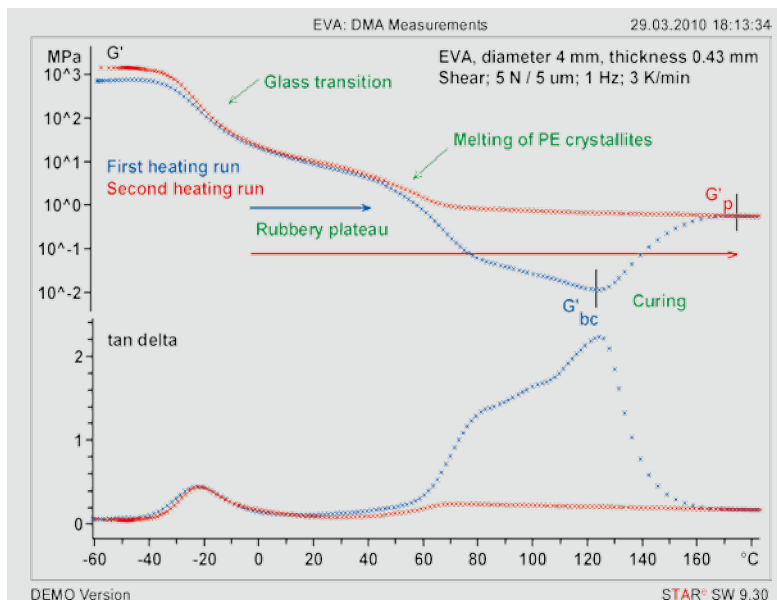


Figure 6. DMA measurements showing first (blue) and second (red) heating runs.

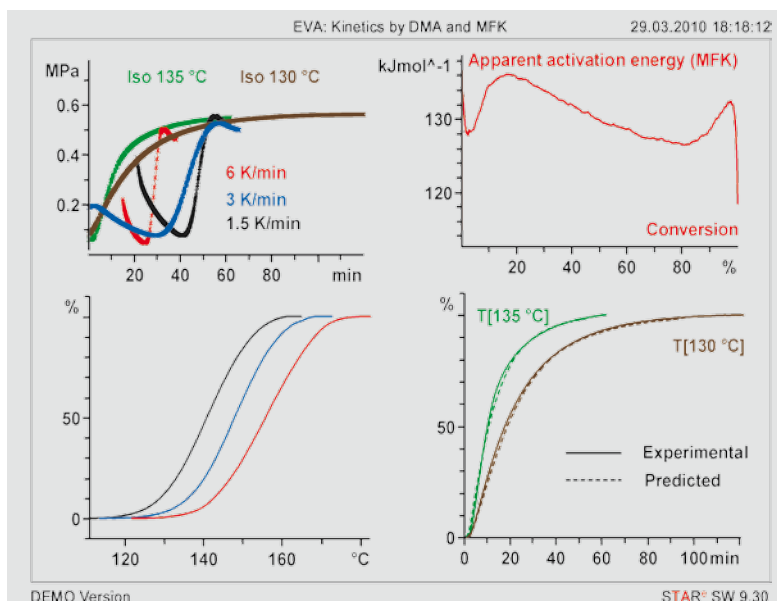


Figure 7. DMA/MFK evaluation. Above left: dynamic and isothermal DMA curves. Below left: conversion curves. Above right: the apparent activation energy. Below right: predictions for isothermal curing at $130\text{ }^{\circ}\text{C}$ and $135\text{ }^{\circ}\text{C}$ and the corresponding experimental measurements.

difference between the plateau modulus, G'_p , (170 °C at a heating rate of 3 K/min) and the modulus before curing:

$$\alpha(T) = \frac{G'(T) - G'_{bc}}{G'_p - G'_{bc}}$$

The conversion curves determined from the dynamic measurement curves are shown in Figure 7 (below left). These curves were used to calculate the conversion-dependent activation energy (see Figure 7, above right). From this, isothermal predictions were derived for 130 and 135 °C (Figure 7, below right). For comparison, the diagram also shows the conversion curves obtained from isothermal experiments performed at the same two temperatures. The measured curves are shown in Figure 7, above left. The measured and calculated conversion curves again show excellent agreement.

Figure 8 compares the results obtained from DSC kinetics with those from DMA

kinetics. The figure shows that the calculated activation energy is of the same order of magnitude for both techniques. Furthermore, for curing times longer than 10 min, it is apparent that the degree of cure determined by DMA is higher than the values obtained from the DSC measurements.

The reason for this is that we have assumed that the plateau modulus is independent of temperature (the modulus is needed for the calculation of the DMA conversion curve).

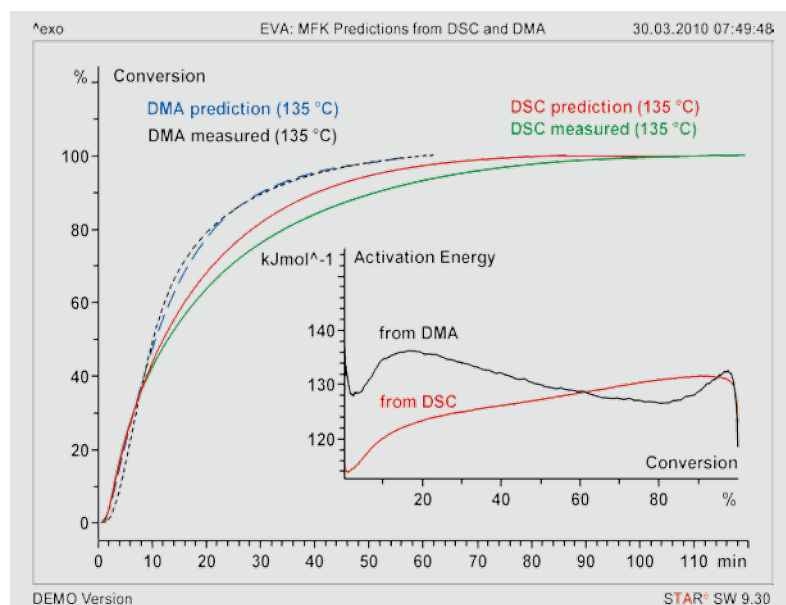
However, Figure 6 shows that G' decreases slightly with increasing temperature in the rubbery plateau and the calculated degree of cure is therefore somewhat too large (see the G' curve in the second heating run). Quantitative estimates show that this effect overestimates the degree of cure determined from the DMA measurements by not more than 10%.

Conclusions

The kinetics of the curing reaction of EVA that occurs during the lamination of photovoltaic modules can be investigated using DSC and DMA measurements. This is done by performing measurements at different heating rates and evaluating the results using the model free kinetics method. The results show that both techniques can be used to describe the curing process of EVA. The predictions made from model free kinetics about the isothermal curing behavior were confirmed experimentally. Both DSC and DMA measurements are suitable for the optimization of process parameters for the lamination of photovoltaic modules. DMA yields additional information with regard to the viscoelastic behavior of the EVA film in the finished photovoltaic modules.

The two techniques can be equally well used for the quality control of laminated photovoltaic modules.

Figure 8. Comparison of DMA and DSC results and MFK evaluation. Activation energy and predictions for isothermal temperatures and comparison with isothermal measurements.



References

- [1] Michael DeBergalis, *Journal of Fluorine Chemistry* 125 (2004), 1255–1257.
- [2] T. Krieger, H. Roekens-Guibert, *Environmental impacts of Tedlar® PVF film for use in photovoltaic modules*, DuPont.
- [3] A. K. Plessing, in: G. M. Wallner, R.W. Lang (Eds.), *Proceedings of Polymeric Solar Materials*, Leoben, Austria, 2003, pp. XIII–XIII8.
- [4] Z. Xia, D.W. Cunningham, *J.H. Wohlgemuth, PV Modules*, 5, 1(2009), 150–159.
- [5] *Tips on model free Kinetics*, UserCom 8, 1–3.
- [6] Jürgen Schawe, *Kinetic studies of complex reactions*, UserCom 18, 13–16.

UV curing of a cycloaliphatic epoxy resin using TOPEM® and conventional DSC

Dr. Markus Schubnell

The curing of materials with (ultraviolet) light is often performed at relatively low temperatures, for example even at room temperature. Under these conditions, the material can vitrify. Depending on the temperature, curing slowly continues in the glassy state. The article shows how these processes can be investigated using TOPEM® and conventional DSC measurements.

Introduction

UV-curing paints and varnishes, coatings, and adhesives are nowadays widely used. The main practical advantages of such systems are that they cure within a few seconds and produce high quality coatings at relatively low temperatures (even at room temperature) so that the substrate is subjected to only low levels of thermal stress. In addition, there are important ecological advantages, for example no solvent emission and no drying processes with consequent energy consumption.

Difficulties arise only with the curing of pigmented paints and varnishes because the pigments also absorb UV light, which can lead to incomplete curing.

In this article, we show how isothermal curing processes of light-curing resins can be measured by DSC. We investigated the influence of temperature on the degree of cure determined from dynamic postcuring experiments. Furthermore, using TOPEM®, we describe the behavior of the resin immediately after exposure to the UV light.

Experimental details

The resin chosen for this study was the aliphatic epoxy resin UVR-6107 (Dow) to which a cationic photoinitiator UVI-6976 (Dow) was added to promote rapid crosslinking under UV light. This resin is mainly used for coating metals and as an overprint varnish.

The measurements were performed using a METTLER TOLEDO DSC 1 equipped with a photocalorimeter accessory that allows a sample to be exposed to UV light

for certain times [1]. The measurements were performed in open 40- μ L aluminum crucibles. The sample mass was typically about 7 mg. The light intensity was about 400 mW/cm². Three different types of measurements were performed.

1. Determination of the degree of cure at different temperatures: The sample was first heated to the desired curing temperature and allowed to stabilize for 3 minutes. The UV light source was then switched on and the sample exposed to UV light for 4 minutes. The sample was then held for a further 6 minutes at the curing temperature and again exposed to UV light for a further 4 minutes. Finally, the cured sample was heated twice from 30 °C at a heating rate of 10 K/min.
2. Dynamic postcuring experiments using TOPEM®: The sample was first cured with UV light as described above under 1. The postcuring enthalpy was then measured in a

TOPEM® experiment at a heating rate of 0.8 K/min.

3. Investigation of the curing behavior at different temperatures using TOPEM®: The isothermal “aging behavior” of the samples after exposure to UV light was investigated by increasing the measurement time to 4 hours after UV exposure.

Results

Determination of the degree of cure of the sample after UV exposure using conventional DSC

Figures 1 and 2 summarize the measurement results. Figure 1 shows the results of isothermal measurements with UV light at different curing temperatures. The measurement curves shown are difference curves between the first and second exposures, shown in the example in the upper right diagram in Figure 1. The peak area corresponds to the reaction enthalpy (ΔH_{UV}) produced in the cur-

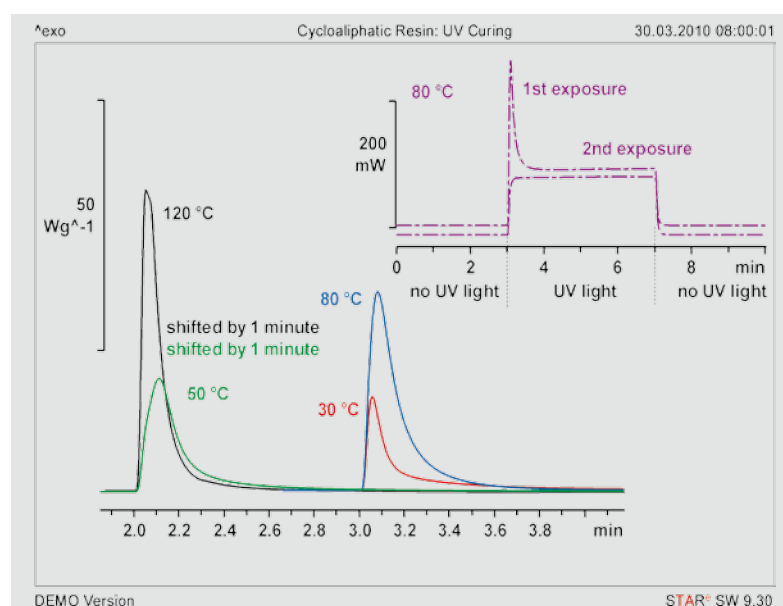


Figure 1. Small coordinate system: DSC curves during the first and second UV exposures at 80 °C. Large coordinate system: Difference curves between first and second exposures at different temperatures. For clarity, the curves for 50 °C and 120 °C were shifted by 1 min to the left.

What is vitrification?

During curing, the resin molecules form bonds and link together. This gives rise to a network and the physical properties of the material changes – the resin is in the liquid state before switching on the UV light source but is partially crosslinked after UV exposure.

At the beginning of the curing reaction, the rate is controlled by the kinetics of the chemical reaction. As the reaction proceeds, the degree of crosslinking increases and the glass transition temperature of the system increases.

When the momentary glass transition temperature reaches the sample temperature (which is equal to the reaction temperature), the material vitrifies. From this time onward, the rate of the curing reaction is limited by the mobility of the reaction participants and not by the kinetics of the reaction.

The mobility of the molecules involved in the reaction is severely restricted through vitrification and the curing reaction practically stops [2, 3].

ing reaction under the action of the UV light. The curves indicate that the reaction is practically complete after about 0.5 minutes. The high rate of reaction results in large maximum heat flows, for example at 120 °C almost 400 mW. These high heat flows (and the reaction enthalpy) lead to a short-term increase in the temperature of the sample during the reaction. For example, in the experiment at 120 °C, the temperature increase was about 15 K. The curves show that the reaction enthalpy (ΔH_{UV} , peak area) becomes larger with increasing temperature.

Figure 2 shows the results of heating measurements performed on the UV-cured samples. The peak area corresponds to the reaction enthalpy of thermal postcuring, ΔH_{PC} . One immediately sees that the postcuring enthalpy, ΔH_{PC} , of the samples cured at low temperatures is significantly larger than that of the samples cured at higher temperatures. Furthermore, the curves differ in shape and in their location on the temperature axis. It is apparent that thermal postcur-

ing begins at about the temperature at which the light curing was performed. This indicates that the material vitrifies during the light curing.

The degree of cure, α_c , after UV exposure can be calculated from the ratio of the reaction enthalpy produced during UV exposure (ΔH_{UV}) and the total enthalpy involved in the curing reaction ($\Delta H_{PC} + \Delta H_{UV}$):

$$\alpha_c = \frac{\Delta H_{UV}}{\Delta H_{UV} + \Delta H_{PC}}$$

The values for ΔH_{UV} and ΔH_{PC} and α_c are summarized in Table 1. The total reaction enthalpy is independent of the curing temperature taking into account the measurement accuracy.

Measurement of the curing behavior using TOPEM®

Figure 2 shows that no glass transition appears to be visible at the beginning of the postcuring peak. The reason for this is that the exothermic postcuring reaction and the glass transition step overlap. It should however be possible to separate the two effects and measure the glass transition using TOPEM®. The results of such an experiment are for example shown in Figure 3 for a sample that had been UV cured at 80 °C. A heating rate of 0.8 K/min and a pulse height of 0.3 K were used. During the first heating run (red curves), the exothermic postcuring reaction can be seen in the non-reversing heat flow curve from about 50 °C onward. The postcuring enthalpy determined from this agrees well with the value calculated from the conventional DSC experiment (Table 1 and Figure 2).

In the corresponding specific heat capacity curve (upper diagram) the slope of the heat capacity changes from about 50 °C onward. This can be understood by assuming that at this low heating rate the material devitrifies from about 50 °C onward and undergoes slow postcuring. As a result, the glass transition temperature shifts to higher temperatures, which leads to the broad, step-like increase in the heat capacity. In the second heating run (blue curves), no postcuring is visible in the non-reversing heat flow curve.

Figure 2. Thermal postcuring experiments performed with the light-cured samples.

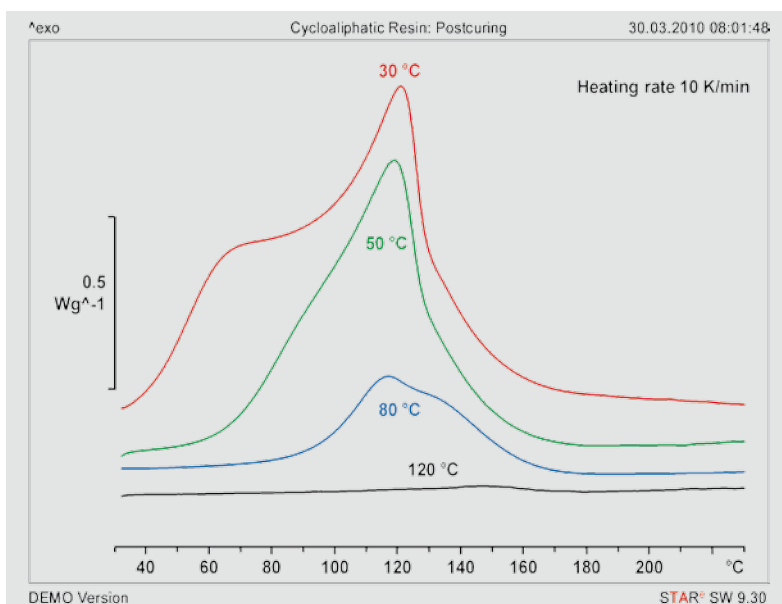


Table 1. Evaluation of the reaction peaks in Figures 1 and 2 and the resulting degree of cure after light curing at different temperatures.

Curing temperature in °C	Light curing ΔH_{UV} in J/g	Thermal postcuring ΔH_{PC} in J/g	Total curing enthalpy in J/g	Degree of cure after light curing in %
30	154	324	479	32
50	275	215	490	56
80	390	75	465	84
120	483	5.6	489	99

In the heat capacity curve, the glass transition temperature of the cured material can be clearly seen at about 153 °C. The heat capacities measured before and after the glass transition during the first and second heating runs agree well with each other.

In order to investigate the behavior of the resin immediately after vitrification, the curing process was studied at different temperatures using TOPEM®. The curves in Figure 4 show the quasi-static heat capacity as a function of time at curing temperatures of 30 °C, 50 °C and 80 °C. The heat capacity curve exhibits large erratic deflections during the UV exposure time. The reason for this is that the stationarity and linearity of the system is not fulfilled under these conditions.

The TOPEM® results cannot therefore be interpreted during UV exposure. What should be compared is the heat capacity before and after exposure of the sample to UV light. Figure 4 shows that there is a marked step-like decrease in the heat capacity after UV exposure, which is typical for vitrification. Furthermore, the heat capacity does not remain constant after the step but decreases further at low curing temperatures and increases at high curing temperatures. If the same experiment is repeated a second time, the step in the heat capacity is no longer observed (see upper blue dashed curve in Figure 4).

How can this behavior be explained? – In fact, after light curing, two processes occur in the partially cured resin:

1) Further crosslinking of the resin:
During UV exposure, a large number of reactive cations are produced in the sample. Vitrification severely restricts the mobility of the resin molecules and the crosslinking practically stops.

At low reaction temperatures, (T_R), the crosslinking reaction has hardly begun when vitrification occurs. It follows that a large number of cations are available. The cations are still able to move in the glassy state so that the reaction continues slowly. Through this, the enthalpy-tem-

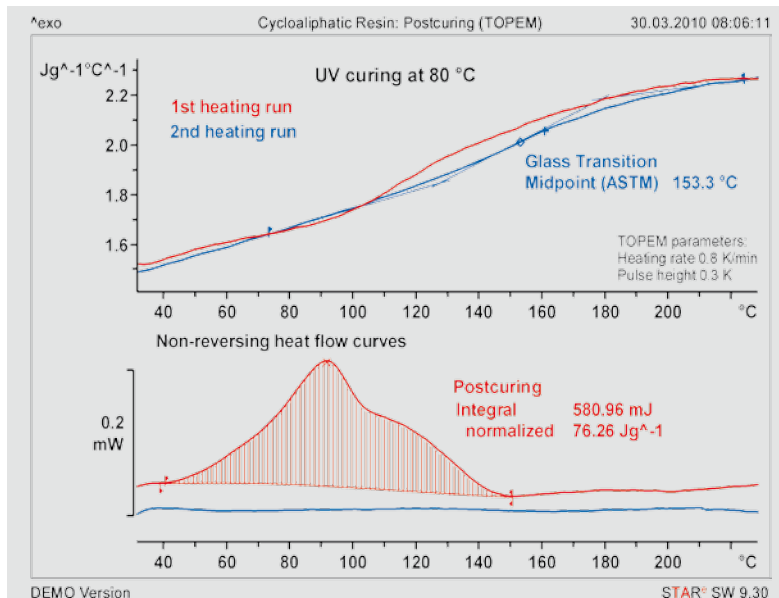


Figure 3. Measurement of a sample after exposure to UV light at 80 °C using TOPEM®.

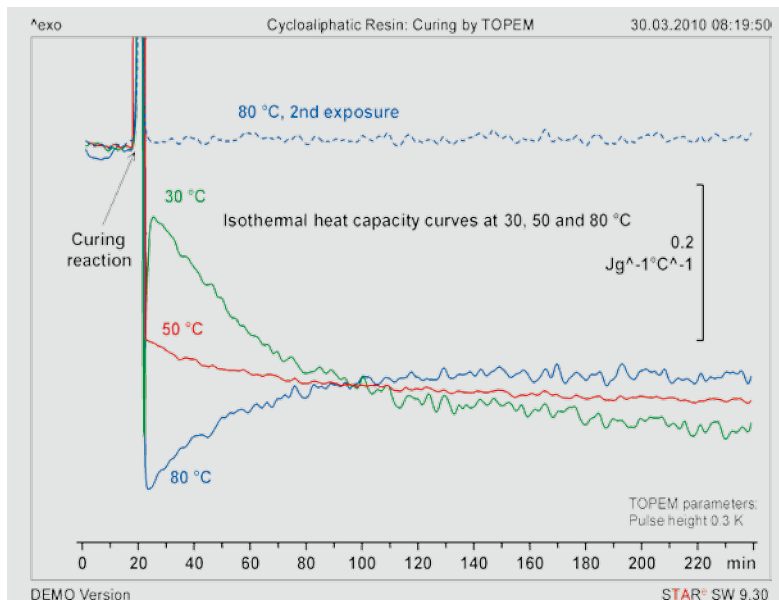


Figure 4. Curves measured by TOPEM® showing the heat capacity of samples cured at different temperatures. After 20 min, the UV light was switched on for 2 min.

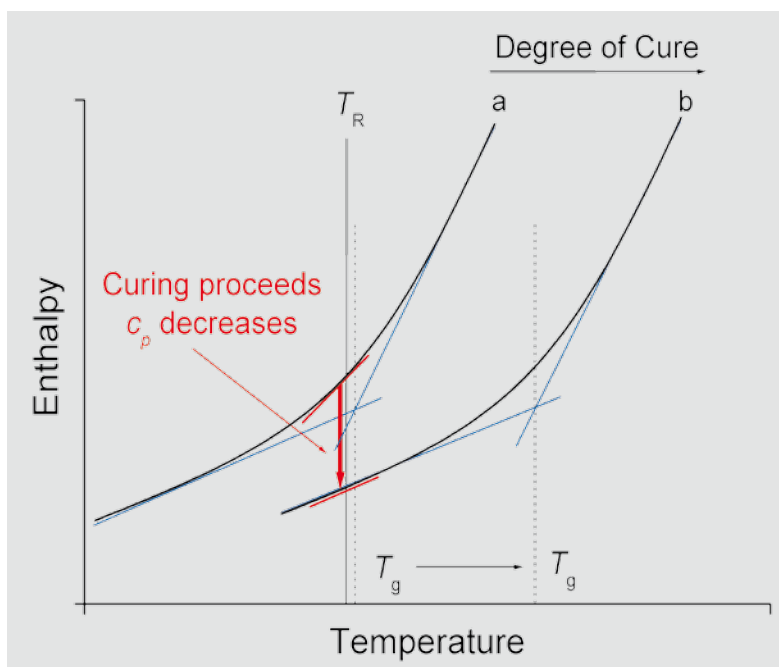


Figure 5. Enthalpy curves for a slightly cured resin (a) and for a more fully cured resin (b). Due to postcuring, the glass transition temperature, T_g , moves further and further away from the reaction temperature, T_R – the heat capacity decreases.

perature function of the resin (Curve a in Figure 5) shifts to higher temperatures (Curve b in Figure 5). The reaction temperature remains constant (isothermal experiment). The result of this process is that the heat capacity (= the slope of the enthalpy curve of the resin) decreases.

2) "Aging" of the resin:

The light curing of the resin corresponds to a cooling experiment performed at a

very high cooling rate. The reaction temperature, T_R , is only slightly lower than the glass transition temperature, the material is not in thermodynamic equilibrium ($T_R \sim T_g$). The sample therefore relaxes relatively quickly. This relaxation process leads to an increase in the specific heat capacity (Figure 6). If aging occurs at a temperature $T_R \ll T_g$, the change in heat capacity during aging can be neglected.

At low temperatures (e.g. at 30 °C) the first of the two processes dominates; at high temperatures (e.g. at 80 °C) the second. At temperatures in between (e.g. at 50 °C), the two processes more or less balance one another.

Conclusions

Light-curing reactions take place within seconds. At low curing temperatures in particular, vitrification of the system usually occurs. The curing process is however often not complete and the material is not in a stable state.

Measurements using TOPEM® have shown that the epoxy resin investigated here only reaches a stable final state about two hours after light curing.

References

- [1] M. Schubnell, Curing of powder coatings using UV light, UserCom 19, 13–16.
- [2] J. Schawe, Kinetic studies of complex reactions. Part 1: Model free kinetics, UserCom 18, 13–16.
- [3] J. Schawe, Kinetic studies of complex reactions. Part 2: Description of diffusion control, UserCom 19, 8–10.

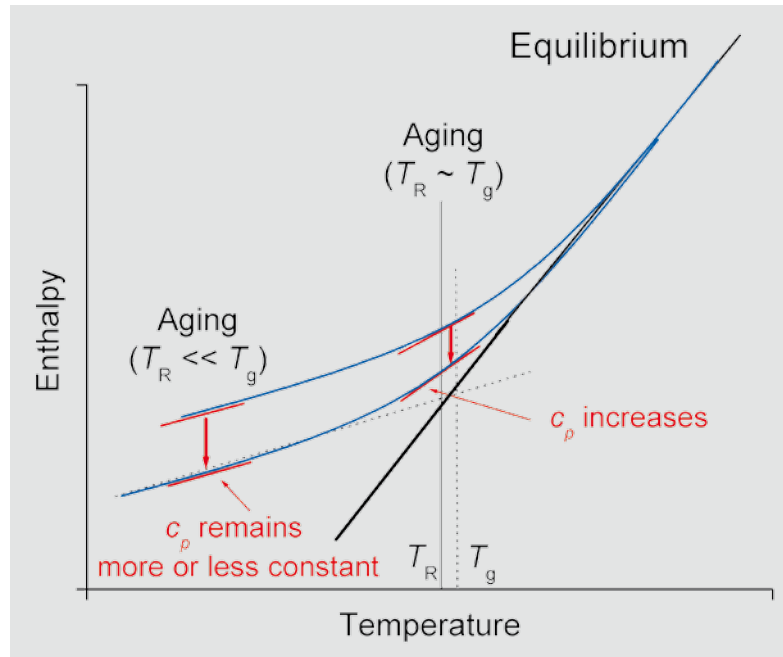


Figure 6. After vitrification, $T_R \sim T_g$. Under these conditions, the sample ages relatively quickly; the specific heat capacity increases. If the aging occurs at a temperature $T_R \ll T_g$, the change in heat capacity during aging can be neglected.

Analysis of the components of a sandwich composite panel by DMA

Ni Jing

The mechanical properties of the individual components of a sandwich composite panel were investigated by DMA. The temperature-dependent shear moduli of the polyurethane foam core and the bending modulus of the carbon fiber epoxy composite skin sheets are important quantities that determine the mechanical behavior of the sandwich construction.

Introduction

A sandwich composite panel consists of a lightweight core sandwiched between two thin, stiff skin sheets. Sandwich structures of this type are often employed when products have to exhibit high bending strength and stiffness but at the same time need to be light in weight. Typical examples of successful industrial applications are the wing flaps of aircraft, wind turbine blades, surfboards, and boat superstructures.

Figure 1 shows a typical sandwich composite panel. When a bending load is applied, the skin sheets experience compressive or tensional stresses. They absorb the major part of the forces within the sandwich construction and are responsible for its high bending strength. The core must withstand shear stresses and compression. It supports and stabilizes the skin sheets so that they stay fixed in place relative to one another and do not buckle (deform). The material properties and geometries of the core and skin sheets are the most important factors that determine the strength and stiffness of such sandwich composite panels.

Information about the shear modulus of a potential core material in the temperature range in which the product is expected to be used is necessary in order to choose a suitable material and assess the mechanical properties of the sandwich structure. A soft core made of a material with a low shear modulus is easily deformed and the skin sheets would only be capable of absorbing a small amount of stress. A sandwich structure like this would be weak, too flexible, and easily

deformed. A core material that cannot withstand a certain amount of shear stress is therefore unsuitable.

When a core material with a relatively high shear modulus is used, the skin material takes up the bending stresses in such a way that the forces act as tensional or compressive stresses. Materials commonly used for cores are rigid foams (polyurethane, PVC, polystyrene), wood (balsa and cedar) or honeycomb structures (aluminum, PE, PP).

Similarly, knowledge of the Young's modulus and temperature behavior of the skin sheets is important. A strong skin sheet with high Young's modulus can absorb far more tensional and compressive

stress than the core and makes the sandwich construction much stiffer. Glass or carbon fiber reinforced composites are often used as skin sheets.

The skin and core materials should be balanced with regard to their mechanical properties – the material stress should be shared so that neither part prematurely fails. This applies not only at room temperature but also over the entire temperature range of the application. Softening of a material or major transitions should not occur in the application range.

This article describes how the individual components of the sandwich construction (skin sheets and core) were measured by dynamic mechanical analysis, DMA.

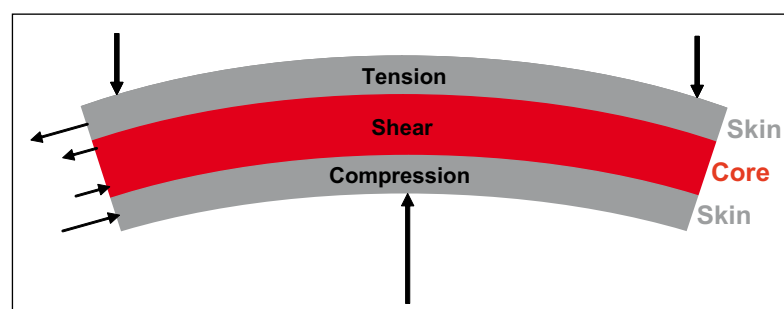


Figure 1. A sandwich structure with bending stress applied at right angles to the panel.

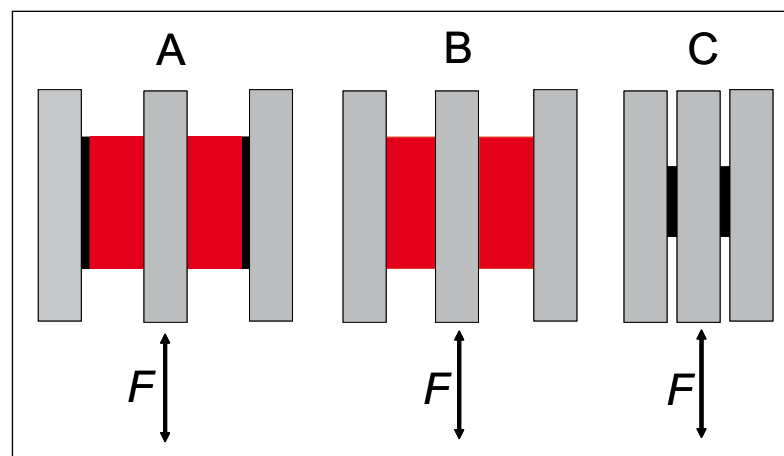


Figure 2: Sample arrangements for the shear measurements. A: a two-layer structure of one skin and the core, B: only the core, C: only the skin sheet.

Experimental details

The sandwich composite panel consisted of two 0.64-mm thick skin sheets and a 6-mm core made of polyurethane rigid foam. The skin sheets were made of a carbon fiber reinforced epoxy composite. Shear, compression and bending measurements were performed using a METTLER TOLEDO DMA/SDTA861[®] dynamic mechanical analyzer.

Shear measurement

The sample specimens were prepared as shown schematically in Figure 2 and loaded in the shear sample holder.

Sample A:

Two rectangular blocks, 6.3 mm long, 5.1 mm wide and 3.4 mm thick, were

prepared by removing one of the skins. The skin thickness was 0.64 mm and the foam thickness 2.8 mm. The measurement conditions were: heating rate 2 K/min, maximum force amplitude 8 N, maximum displacement amplitude 5 μm . The experiments were performed at 1, 10 and 100 Hz.

Sample B:

Two rectangular blocks, 7.3 mm long, 5.4 mm wide and 4.3 mm thick, were prepared from the core by removing the skin sheets. The measurement conditions were: heating rate 2 K/min, maximum force amplitude 8 N, maximum displacement amplitude 5 μm . The experiments were performed at 1, 10 and 100 Hz.

Sample C:

Two pieces of the skin sheet, 3.5 mm long, 2.0 mm wide and 0.60 mm thick, were cut out and the surfaces polished flat. The measurement conditions were: heating rate 2 K/min, maximum force amplitude 8 N, maximum displacement amplitude 5 μm . The experiments were performed at 10 Hz and 100 Hz.

Determination of Young's modulus

A specimen of the skin sheet (the carbon fiber reinforced epoxy composite) was prepared without the rigid foam core for a 3-point bending measurement. The active length was 35.0 mm, the width 5.9 mm, and the thickness 0.60 mm. The specimen was heated at 2 K/min. A constant predeformation force of 0.2 N applied; the maximum force amplitude was 0.15 N, and the maximum displacement amplitude 20 μm . The measurements were performed at 1 Hz.

The polyurethane rigid foam core was also measured in the compression mode: The specimen was 5.6 mm long, 4.6 mm wide, and 7.3 mm thick. A predeformation offset force of 130% was applied; the maximum force amplitude was 1 N, and the maximum displacement amplitude 5 μm . The measurements were performed at 1 Hz.

Results and discussion

Shear measurements

Figure 3 shows the storage modulus (G'), the loss modulus (G'') and the loss factor ($\tan \delta$) of a sample measured in the shear mode. A secondary relaxation effect is observed at about -30°C as a small step in G' or as a broad peak in G'' and $\tan \delta$. The temperatures of these peaks depend on the frequency and lie between about -43°C for 1 Hz and -24°C for 100 Hz. The glass transition is at 100°C is also frequency dependent.

In the curve measured at 1 Hz, the $\tan \delta$ peak clearly exhibits a shoulder at about 80°C . The shoulder is still visible in the curve measured at 10 Hz. It indicates that two effects overlap and cannot be separated when the core and skin sheet are measured together. To understand

Figure 3. DMA curves of the shear measurement of sample A.

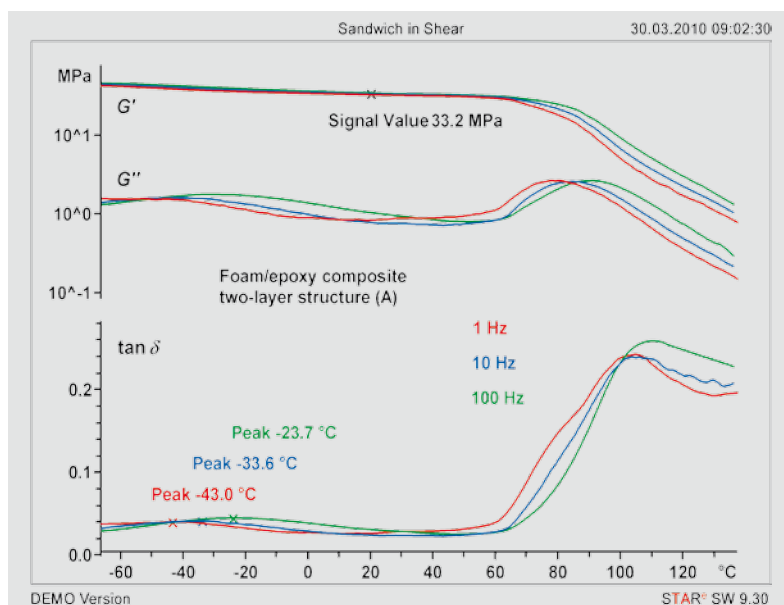
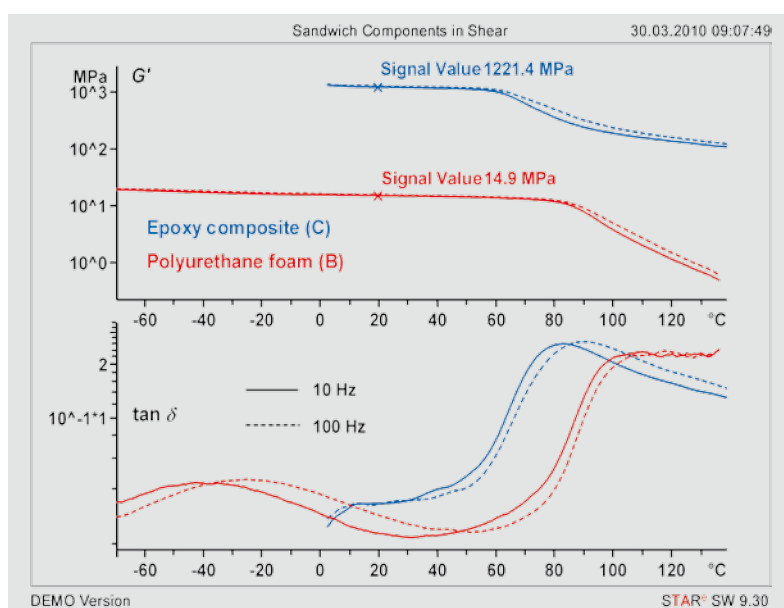


Figure 4: Shear measurements of samples B and C.



this behavior better, the two components were measured separately.

Figure 4 shows the DMA curves of the individual components B and C of the sandwich construction measured in the shear mode at 10 and 100 Hz. Here again, a broad relaxation effect can be seen at around $-35\text{ }^{\circ}\text{C}$ (10 Hz) and a glass transition at about $100\text{ }^{\circ}\text{C}$. Both effects can be assigned to the core material (polyurethane, Sample B). The skin sheet (epoxy composite, Sample C) exhibits a glass transition at about $80\text{ }^{\circ}\text{C}$. The two glass transitions are close to one another. The two-layer structure (Sample A) measured in Figure 3 shows stable modulus properties up to about $60\text{ }^{\circ}\text{C}$.

As was to be expected, the shear modulus of the relatively soft polyurethane core is much smaller than that of the epoxy composite skin sheet. The soft component therefore dominates in the shear measurement [1]. The value of G' (33.2 MPa) for Sample A is not much larger than that of Sample B (14.9 MPa).

Determination of Young's moduli

The Young's moduli of the individual components (skin sheet and core) were measured by 3-point bending (epoxy composite) and compression (polyurethane). The rigid foam is too soft to be measured in the bending mode but is ideal for measurement in compression.

The course of the DMA curves shown in Figure 5 is similar to the curves measured in the shear mode. The values of the storage moduli, E' , are however much larger. For the isotropic foam, we obtain a fac-

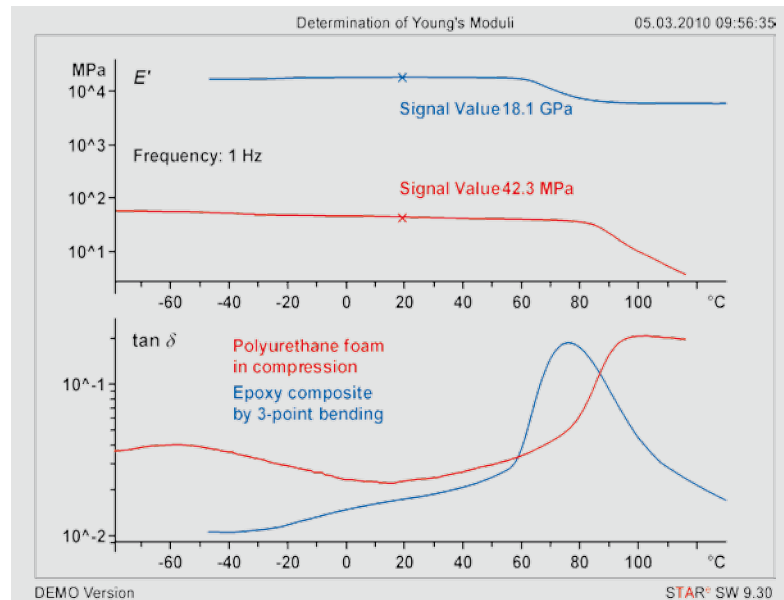


Figure 5. Determination of the Young's moduli of the individual components at 1 Hz.

tor of 3 ($G' = 14.9\text{ MPa}$, $E' = 42.3\text{ MPa}$), which corresponds to a Poisson ratio of 0.5 [2]. Since the epoxy composite material is anisotropic, the Poisson ratio deviates significantly from 0.5.

The peak temperatures are also lower than those observed in the shear measurements because this measurement was performed at 1 Hz. The epoxy composite shows a further relaxation process in the range $-30\text{ }^{\circ}\text{C}$ to $40\text{ }^{\circ}\text{C}$, which is observed as a broad shoulder in the $\tan\delta$ curve.

Conclusions

The mechanical properties and the performance of sandwich constructions are mainly influenced by the properties of the core and the skin sheets. The shear and Young's moduli are easy to measure by DMA over a large temperature range.

Rigid polyurethane foam is used as core material and is capable of withstand-

ing the shear stresses in the sandwich construction. Nevertheless, the shear storage modulus, G' , (14.9 MPa) is relatively small. In contrast, the bending modulus, E' , of the skin sheet is large (18.1 GPa). This allows the desired stiffness of the sandwich panel to be achieved and at the same time with a lightweight structure.

The glass transitions of the two components are close to one another, between $80\text{ }^{\circ}\text{C}$ and $100\text{ }^{\circ}\text{C}$. The sandwich panel can therefore be used up to about $60\text{ }^{\circ}\text{C}$ without loss of strength because the moduli are more or less constant up to this temperature.

References

- [1] Jürgen Schawe, Optimum choice of method and evaluation in DMA measurements of composites, UserCom 26, 1–4.
- [2] Georg Widmann, Interpreting DMA curves, UserCom15, 1–6.

TGA/MaxRes used for studies on hydrogen storage

R. Chiriac¹, C. Sigala¹, J. Andrieux¹, L. Laversenne¹, C. Goutaudier² et P. Miele¹

Université de Lyon, ¹Laboratoire de Multimatiériaux et Interfaces, CNRS UMR 5615

²Laboratoire Hydrazines et Procédés, CNRS UMR 5179, 69622 Villeurbanne Cedex, France

The production of energy from renewable sources is usually subject to fluctuations and requires intermediate storage systems. Hydrogen is a particularly promising possibility. One field of research is focused on developing ways to make hydrogen safe to use by storing it in suitable solids. Borohydrides show great potential. Hydrogen can be regenerated through controlled reaction with water. This produces hydrates of different composition. The following article shows how TGA can be used to study the stability ranges of the hydrates. This information is important for optimum process control and for obtaining a high yield of hydrogen.

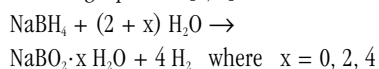
Introduction

Renewable energies such as solar energy, wind energy or biomass are crucial to solving the energy crisis and providing a sustainable supply of energy.

A major difficulty with renewable forms of energy is that they are not continuously available (e.g. the day and night cycle with solar energy). To bridge gaps in supply, renewable energy forms have to be somehow temporarily stored. Hydrogen is a particularly promising candidate for this purpose. It can be generated electrolytically from water and converted to electricity as needed in a fuel cell thereby producing water once again. Hydrogen is thus a form of energy that can be stored and transported.

Hydrogen can in fact be stored and transported as a gas, as a liquid or bound in a solid. Due to safety regulations, its storage as a gas or liquid is rather difficult and expensive.

For this reason, research is focused on the storage of hydrogen in solids, for example as metal or complex hydrides [1]. The latter includes sodium borohydride, NaBH₄. This material can store up to 10.6 mass% hydrogen. Hydrogen is regenerated from the hydride through the controlled addition of water according to the following equation [2, 3]:



The percentage yield of hydrogen depends on the degree of hydration x of the metaborate produced. For example, the hydrates bind additional water molecules that are then no longer available to generate hydrogen. The maximum hydrogen capacity is 10.6% if the anhydride is formed ($x = 0$), but only 5.5% if the tetrahydrate ($x = 4$) is formed. These calculations refer to the hydrogen that is produced from the sum of the reactants (sodium borohydride and water, see Table 1). For mobile applications in particular, the weight of water that has to be transported is important.

The aim of our research is to determine the different hydrate steps of the metaborate using thermogravimetric analysis (TGA) and in particular the MaxRes method. This information is important for defining the experimental conditions to ensure that only hydrates with relatively low degrees of hydration occur when hydrogen is generated from the sodium borohydride.

TGA measurements are usually performed at constant heating rates. However, low heating rates and correspondingly long measurement times are essential for achieving pseudo-equilibrium conditions and hence optimum resolution of the TGA steps.

Different techniques have been developed in the past decades to keep measurement

times as short as possible. These involve varying the heating rate under control during the measurement [4–8].

MaxRes, is an event-controlled technique developed by METTLER TOLEDO in which the momentary heating rate is controlled by the rate of loss of mass (DTG). The most important control parameters are [8]:

- Maximum and minimum heating rate, v_{max} and v_{min}
- Threshold values for switching the heating rate based on the DTG signal: S_{high} to lower the rate and S_{low} to increase it.

These parameters can be optimized to achieve both good separation of the weight loss steps and short analysis times.

This article describes how the stability ranges of the different hydrate steps of NaBO₂ are identified and characterized using MaxRes.

Experimental details

Substance: NaBO₂·4H₂O from ACROS ORGANICS (after grinding, written as NaBO₂· x H₂O).

Sample preparation: the material was finely ground in a mortar at room temperature.

Measurement system: METTLER TOLEDO STAR[®] System, TGA/SDTA 851[°] with 1600 °C furnace.

Crucible: 100- μ L aluminum with pierced lid (diameter of hole about 670 μ m).
 Sample weight: approx. 16 mg.
 Temperature program: 25 to 340 $^{\circ}$ C at different heating rates.
 Furnace atmosphere : 40 mL/min air.
 MaxRes parameters: v_{max} and v_{min} and S_{high} and S_{low} : see Results and discussion.

Results and discussion

Figure 1 shows the dehydration steps of $\text{NaBO}_2 \cdot x\text{H}_2\text{O}$ measured at heating rates between 0.1 and 5 K/min. The resolution of the steps is clearly better at low heating rates. The weight loss step at 80 $^{\circ}$ C depends not only on the stoichiometric composition but also on the moisture content of the sample material. Since the weight loss steps between 90 and 140 $^{\circ}$ C are not well separated, it is not possible to determine the individual hydrate steps even at the lowest heating rate of 0.1 K/min.

The MaxRes method was then used to improve the identification of the individual hydrate phases. Several experiments were necessary to optimize the method with regard to separation of the steps and duration of the measurement. Figure 2 shows three measurement curves performed using different MaxRes parameters. The resulting measurement times are also given. The best resolution of the hydrate steps is shown in Curve B; the measurement time was about 6 h. The measurement at a constant heating rate of 1 K/min (Figure 1) lasts about the same time (5 h), but does not resolve the steps so well. Only the very slow measurement at 0.1 K/min results in comparable resolution – the measurement time is however ten times longer.

The parameters given for MaxRes in Figure 2 show that the threshold values used for the switching levels (S_{high} and S_{low}) are very important: the tendency is that smaller values provide better resolution (compare curves B and C). The maximum heating rate also has an important influence on the separation and the measurement time. Curve B shows better resolution than curve A, although A was measured at a lower v_{max} (1 K/min)

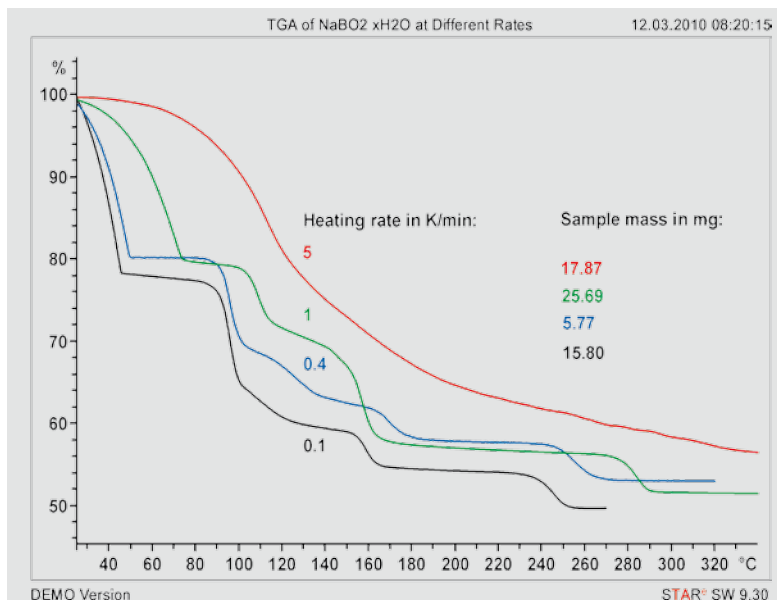


Figure 1. TGA curves of $\text{NaBO}_2 \cdot x\text{H}_2\text{O}$ measured at different constant heating rates.

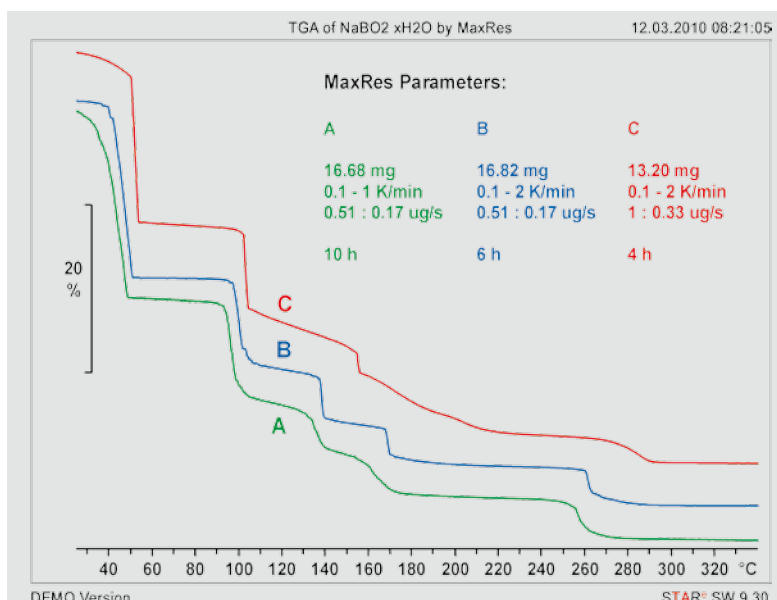


Figure 2. MaxRes curves of $\text{NaBO}_2 \cdot x\text{H}_2\text{O}$ measured with different parameters v_{min} – v_{max} in K/min and S_{high} : S_{low} in μ g/s. This results in different measurement times.

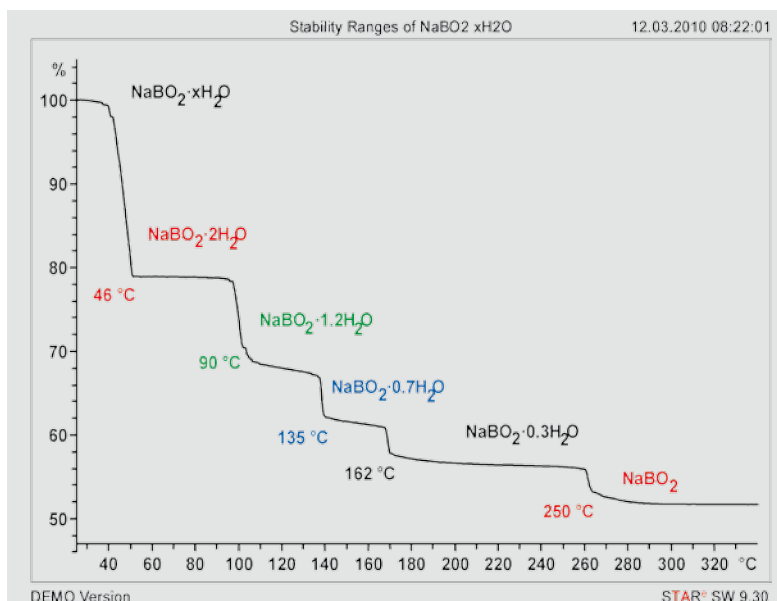


Figure 3. Stability ranges of the hydrates of the metaborate. The starting material, $\text{NaBO}_2 \cdot x\text{H}_2\text{O}$, was a mixture of $\text{NaBO}_2 \cdot 4\text{H}_2\text{O}$ and $\text{NaBO}_2 \cdot 2\text{H}_2\text{O}$.

than B (2 K/min). The best results were achieved using the following combination of parameters:

$$v_{\max} = 2 \text{ K/min}, v_{\min} = 0.1 \text{ K/min}, \\ S_{\text{high}} = 0.51 \text{ } \mu\text{g/s}, S_{\text{low}} = 0.17 \text{ } \mu\text{g/s}.$$

The MaxRes method allows the different hydrate steps of the metaborate to be separated and their stability range to be characterized (Figure 3). The following hydrates were confirmed by X-ray analysis:

$\text{NaBO}_2 \cdot 4\text{H}_2\text{O}$, $\text{NaBO}_2 \cdot 2\text{H}_2\text{O}$, and $\text{NaBO}_2 \cdot 0.3\text{H}_2\text{O}$ with the temperatures for further dehydration of 46 °C, 90 °C and 250 °C (Table 1).

The two newly observed phases $\text{NaBO}_2 \cdot 1.2\text{H}_2\text{O}$ and $\text{NaBO}_2 \cdot 0.7\text{H}_2\text{O}$ have not been previously described. In further studies, the next step would be to inves-

tigate whether these phases are stable compositions or whether they are metastable.

Summary and conclusions

The well-known hydrates of NaBO_2 were identified and their thermal stability ranges characterized using the MaxRes method. In addition, two previously unknown hydrates were found. Since borates can form metastable states, it can be assumed that the event-controlled dehydration (MaxRes method) favors the formation of such states. Knowledge of the stability ranges of the different hydrates helps one to optimize the hydrolysis of sodium borohydride. When sodium borohydride is used as a storage medium to generate hydrogen through reaction with water, the degree of hydration of the resulting NaBO_2 should be as low as possible.

Table 1.
Yield of hydrogen with the different NaBO_2 hydrates and their dehydration temperatures.

Degree of hydration	Yield of hydrogen in mass%	Dehydration temperature (°C)
NaBO_2 anhydride	10.8	–
$\text{NaBO}_2 \cdot 0.3\text{H}_2\text{O}$	10.0	250
$\text{NaBO}_2 \cdot 2\text{H}_2\text{O}$	7.3	90
$\text{NaBO}_2 \cdot 4\text{H}_2\text{O}$	5.5	46

References

- [1] A. Züttel, Hydrogen storage methods, *Naturwissenschaften*, 91 (2004) 157.
- [2] H. I. Schlesinger, H. C. Brown, A. E. Finholt, J. R. Gilbreath, H. R. Hoekstra and E. K. Hyde, Sodium borohydride, its hydrolysis and its use as a reducing agent and in the generation of hydrogen, *J. Am. Chem. Soc.*, 5 (1953) 215.
- [3] R. Bouaziz, Contribution à l'étude des borates de lithium et de sodium, *Ann. chim. (Paris)*, 6 (1961) 348–93.
- [4] R. Riesen, Adjustment of heating rate for maximum resolution in TGA and TMA (MaxRes), *Journal of Thermal Analysis*, 53 (1998) 365–374.
- [5] J. Rouquerol, Controlled rate evolved gas analysis: 35 years of rewarding services, *Thermochimica Acta*, 300 (1997) 247–253.
- [6] O. T. Sørensen, RCTA techniques used in studies of solid state reactions in inorganic compounds, *Journal of Thermal Analysis and Calorimetry*, 56 (1999) 17–26.
- [7] M. Reading, "Controlled rate thermal analysis and related techniques", Chapter 8 in *Handbook of Thermal Analysis and Calorimetry*, Michael E. Brown, Editor, ISBN 0-444-82085-X, 1998.
- [8] B. Schenker, R. Riesen, MaxRes: Event-controlled adaptation of the heating rate, *UserCom* 6, 10–12.

Exhibitions, Conferences and Seminars – Veranstaltungen, Konferenzen und Seminare

11 th Laehnwitzseminar on Calorimetry	June 6–11, 2010	Rostock, Germany
INTERSOLAR 2010 Trade Fair	June 9–11, 2010	Munich, Germany
50° SIMPOSIO AFI 2010	June 9–11, 2010	Rimini, Italy
ESTAC-10	August 22–27, 2010	Rotterdam, Netherlands
HET Instrument 2010	September 28–October 1, 2010	RAI Amsterdam, Netherlands
Kunststoffmesse «K 2010» International Trade Fair for Plastics and Rubber	October 27–November 3, 2010	Düsseldorf, Germany

International and Swiss TA Customer Courses:

TA Customer Courses and Seminars in Switzerland – Information and Course Registration:

TA-Kundenkurse und Seminare in der Schweiz – Auskunft und Anmeldung:

Ms Esther Palma-Andreato, Ms Perla Irmier, Mettler-Toledo AG, Analytical, Schwerzenbach,
Tel: ++41 44 806 73 57, Fax: ++41 44 806 72 60, e-mail: esther.palma@mt.com or perla.irmier@mt.com

Courses / Kurse

SW Basic (Deutsch)	15. November 2010	SW Basic (English)	November 22, 2010
TMA (Deutsch)	15. November 2010	TMA (English)	November 22, 2010
DMA Basic (Deutsch)	15. November 2010	DMA Basic (English)	November 22, 2010
DMA Advanced (Deutsch)	16. November 2010	DMA Advanced (English)	November 23, 2010
TGA Basic (Deutsch)	16. November 2010	TGA Basic (English)	November 23, 2010
TGA Advanced (Deutsch)	17. November 2010	TGA Advanced (English)	November 24, 2010
DSC Basic (Deutsch)	17. November 2010	DSC Basic (English)	November 24, 2010
DSC Advanced (Deutsch)	18. November 2010	DSC Advanced (English)	November 25, 2010
TGA-FTIR (Deutsch)	18. November 2010	TGA-FTIR (English)	November 25, 2010
SW Advanced (Deutsch)	19. November 2010	SW Advanced (English)	November 26, 2010
TGA-MS (Deutsch)	19. November 2010	TGA-MS (English)	November 26, 2010
Kinetics / TMDSC (Deutsch)	19. November 2010	Kinetics / TMDSC (English)	November 26, 2010

Local TA Customer Courses:

TA-Kundenkurse und Seminare in Deutschland und der Schweiz

Nähere Informationen unter www.mt.com/labtalk oder durch:
Frau Petra Fehl, Mettler-Toledo GmbH, Giessen, Tel: ++49 641 507 404,
e-mail: labtalk@mt.com

Anwenderworkshop DSC (kostenpflichtig)	21. und 22.09.2010	Giessen
Online-Seminare zu div. Themen	div. Termine	www.mt.com/ta-webinars

Cours et séminaires d'Analyse Thermique en France

Renseignements et inscriptions par Christine Fauvarque, Mettler-Toledo S.A., 18–20 Av. de la pépinière, 78222 Viroflay Cedex,
Tél: ++33 1 3097 1439, Fax: ++33 1 3097 1660, e-mail: christine.fauvarque@mt.com

Principe de la TMA/DMA	15 novembre 2010	Viroflay (France)	Principe de la TGA	18 novembre 2010	Viroflay (France)
DSC: notions de base	16 novembre 2010	Viroflay (France)	Logiciel STAR [®] : perfectionnement	19 novembre 2010	Viroflay (France)
DSC: perfectionnement	17 novembre 2010	Viroflay (France)			

TA Basic Courses and Seminars in Benelux

For more details of training courses and seminars, please contact:
Netherlands: Hay Berden, Tel: ++31 344 63 83 63, e-mail: hay.berden@mt.com
Belgium: Philippe Larbanois Tel: ++32 2 477 40 40 36, e-mail: philippe.larbanois@mt.com

DSC Basics	June 15, 2010	MT NL Tiel
DSC Basics	June 16, 2010	MT B Zaventem
Seminar on Cp determination by DSC, TGA/DSCHT, TOPEM	November 9, 2010	

Corsi e Seminari di Analisi Termica in Italia

Per ulteriori informazioni Vi preghiamo di contattare:
Simona Ferrari, Mettler-Toledo S.p.A., Novate Milanese, Tel: ++39 02 333 321, Fax: ++39 02 356 2973, e-mail: simona.ferrari@mt.com

DSC base	8 Giugno 2010	21 Settembre 2010	Novate Milanese
DSC avanzato	9 Giugno 2010	22 Settembre 2010	Novate Milanese
TGA	10 Giugno 2010	23 Settembre 2010	Novate Milanese
TMA	11 Giugno 2010	24 Settembre 2010	Novate Milanese

TA Customer Courses and Seminars in Slovenia

For details of training courses and seminars, please contact:
Keith Racman, Mettler Toledo d.o.o., Tel: +386 1 547 49 04, Fax: +386 1 542 02 52, e-mail: keith.racman@mt.com

Seminar on Thermal Analysis	October 19–21, 2010	Pluj, Slovenia
International Symposium on Temperature, Humidity, Moisture and Thermal Measurements in Industry and Science	May 31–June 4, 2010	Portorož, Slovenia

Cursos y Seminarios de TA en España

Para detalles de los cursos y seminarios, por favor contacte con:
Francesc Català, Mettler-Toledo S.A.E., Tel: ++34 93 223 76 00, e-mail: francesc.catala@mt.com

Aplicaciones del Análisis Térmico	Junio 2010	Barcelona
Operación con los equipos de Análisis Térmico (DSC y TGA)	Junio 2010	Barcelona
Aplicaciones y uso del Análisis DMA	Julio 2010	Bilbao
Aplicaciones del Análisis Térmico	Junio 2010	Madrid
Operación con los equipos de Análisis Térmico (DSC y TGA)	Junio 2010	Madrid

TA Customer Courses and Seminars in the Scandinavian Countries

For details of training courses and seminars, please contact: Fredrik Einarsson, Mettler-Toledo AB, Tel: ++46 455 30 00 80, Fax: ++46 8 6424 562, e-mail: fredrik.einarsson@mtf.com

Scanlab Exhibition	28–30 Sept 2010	Köpenhamn
Termoanalys Infoday	12 Okt. 2010	Köpenhamn 13 Okt. 2010 Göteborg
Termoanalys Infoday	14 Okt. 2010	Oslo 15 Okt. 2010 Stockholm

TA School and Seminars in Korea

For details of training courses and seminars, please contact: HoeWoon Jeong or JungWon Kim at Mettler-Toledo Korea, Tel: ++82 2 3498 3500, e-mail: hoewoon.jeong@mtf.com, jungwon.kim@mtf.com, Web site: www.kr.mtf.com

Thermal Analysis Application Seminars	June 9–11, 2010	Daejeon, Ulsan
Basic & Advanced TA School in 3Q 2010	September 9–10, 2010	Seoul
TA Public Seminars	November 24–26 2010	Seoul, Ulsan
Basic & Advanced TA School in 4Q 2010	December 9–10, 2010	Seoul

TA Courses and Seminars in Taiwan

For details of training courses and seminars, please contact: Karen Chen at Mettler-Toledo Taiwan, Tel: +886-2-26578898 p102; Fax: +886-2-26570776; e-mail: Karen.chen@mtf.com; Web site: www.tw.mtf.com

TGA/DSC 1 同步熱重/熱示差儀原理與應用課程	September 15–16, 2010	台北, 高雄
DSC 操作技術, 曲線解疑與動力學技術課程	November 10–11, 2010	台北, 高雄
熱分析應用 Seminar (彈性材料與熱塑性材料)	August 23–27, 2010	台北, 台中, 高雄

TA Seminars in Thailand

For details of training courses and seminars, please contact: Chatriya Suamsung, Mettler-Toledo (Thailand) Limited, 272 Soi Soonvijai 4, Rama9 Road, Bangkok, Huay Kwang, Bangkok, Thailand 10320
Tel: +66-2-7230338, Fax: +66-2-7196479, e-mail: Chatriya.Suamsung@mtf.com

Thermal Analysis Application Seminar	September 2010	Bangkok, Thailand
--------------------------------------	----------------	-------------------

TA Customer Courses and Seminars in China

For details of training courses and seminars, please contact: Lu LiMing at Mettler-Toledo Instruments (Shanghai) Co. Ltd., Tel: ++86 21 6485 0435, Fax: ++86 21 6485 3351, e-mail: liming.lu@mt.com

TA Public Seminars	June–December 2010	Different cities
TA User Conference	July 20–22, 2010	Shanghai
TA User Training Courses	June–December 2010	Shanghai, Beijing

TA Customer Courses and Seminars in India

For details of training courses and seminars, please contact: Mahesh Tripathi, Mettler-Toledo India Private Limited, Amar Hill, Saki Vihar Road, Powai, Mumbai 400 072
Tel: +91-22-28031 111 / 28031 370, Fax: +91-22-2857 5071, e-mail: mahesh.tripathi@mt.com

Training course	October 2010	Powai, Mumbai
-----------------	--------------	---------------

For further information regarding meetings, products or applications, please contact your local METTLER TOLEDO representative and visit our Web site <http://www.mt.com>

Editorial team

Dr. A. Hammer
Chemist



Ni Jing
Chemist



Dr. D. P. May
Chemist



Dr. R. Riesen
Chem. Engineer



Dr. J. Schawe
Physicist



C. Frisch
Biologist



Dr. M. Schubnell
Physicist



Dr. M. Wagner
Chemist



K. von Euw
Technical Writer



U. Jörimann
Electr. Engineer

Mettler-Toledo AG, Analytical

Postfach, CH-8603 Schwerzenbach

Tel. ++41 44 806 73 87

Fax ++41 44 806 72 60

Contact: urs.joerimann@mtf.com

www.mt.com/ta

For more information